https://doi.org/10.1038/s41556-020-0501-4



Lis1 activates dynein motility by modulating its pairing with dynactin

Mohamed M. Elshenawy^{1,5}, Emre Kusakci², Sara Volz², Janina Baumbach³, Simon L. Bullock[®] and Ahmet Yildiz[®] 1,2,4 ⋈

Lissencephaly-1 (Lis1) is a key cofactor for dynein-mediated intracellular transport towards the minus-ends of microtubules. It remains unclear whether Lis1 serves as an inhibitor or an activator of mammalian dynein motility. Here we use single-molecule imaging and optical trapping to show that Lis1 does not directly alter the stepping and force production of individual dynein motors assembled with dynactin and a cargo adaptor. Instead, Lis1 promotes the formation of an active complex with dynactin. Lis1 also favours the recruitment of two dyneins to dynactin, resulting in increased velocity, higher force production and more effective competition against kinesin in a tug-of-war. Lis1 dissociates from motile complexes, indicating that its primary role is to orchestrate the assembly of the transport machinery. We propose that Lis1 binding releases dynein from its autoinhibited state, which provides a mechanistic explanation for why Lis1 is required for efficient transport of many dynein-associated cargos in cells.

ytoplasmic dynein (hereafter, dynein) is a AAA+ motor responsible for nearly all motility and force generation towards the microtubule (MT) minus-end¹-³. Dynein is involved in a wide variety of cellular functions, such as positioning of intracellular organelles, breakdown of the nuclear envelope and assembly of the mitotic spindle⁴-⁶. The partial loss of dynein function has been implicated in a range of neurodegenerative and neurodevelopmental conditions, including spinal muscular atrophy, amyotrophic lateral sclerosis, Alzheimer's disease, and schizophrenia⁻-⁶.

The core of the dynein complex (1.4 MDa) is a homodimer of two heavy chains¹⁰. The C-terminal motor domain of the heavy chain is a catalytic ring of six AAA modules (AAA1-6). Unlike kinesin, the MT-binding domain of dynein is separated from the catalytic domain by a coiled-coil stalk11. Nucleotide-dependent conformational changes of the linker drive the motility towards the MT minus-end^{12,13}. The N-terminal tail dimerizes the heavy chains¹⁴⁻¹⁶ and binds smaller polypeptides^{1,17,18}. When dynein is not bound to its cargo, it forms two distinct conformations, the phi particle and the open conformation, both of which move poorly along MTs^{19,20}. In the phi conformation, two motor domains self-dimerize through interactions between their linker, AAA+ ring and stalk regions, and dynein interacts weakly with MTs. In the open conformation, the motor domains are more flexible and point towards each other, which is unfavourable for processive motility^{19,21}. Transitions between the phi and open conformations are proposed to be an important part of dynein regulation^{19,21}, but the molecular cues that govern this transition remain unclear.

Recent studies have suggested that dynein and its cofactor dynactin are recruited to cargos through coiled-coil adaptor proteins in a mutually dependent manner²²⁻²⁴ (Fig. 1a). Formation of a dynein-dynactin-cargo adaptor complex aligns the dynein motor domains in a parallel conformation and activates processive motility along MTs^{25,26}. These adaptors recruit dynein to a specific set of cargos^{24,27}, enabling a single dynein gene to be responsible for nearly all minusend directed functions along MTs. BicD2 and BicDR1, members

of the BicD family, are well-characterized coiled-coil adaptors that link dynein to Golgi-derived Rab6 vesicles, as well as nuclear pore complexes and viruses^{26,28,29}. In vitro reconstitution studies have shown that BicDR1 recruits two dyneins to dynactin, whereas the N-terminal coiled-coil domain of BicD2 (BicD2N) mostly recruits a single dynein^{30,31}. Recruitment of two dyneins per dynactin results in complexes assembled with BicDR1 (DDR) moving faster and producing more force than complexes formed with BicD2N (DDB)^{30,32}. The differences elicited by BicD2 and BicDR1 in dynein motility may have a critical role in the sorting of Rab6 vesicles during neuronal differentiation^{23,28}.

Dynein motility is also regulated by Lis1, which directly interacts with the dynein motor domain 33 . Lis1 inhibition reduces the transport of a wide variety of cargos in eukaryotic cells, including endosomes, lysosomes, mRNAs, centrosomes and nuclei $^{34-41}$. The critical role of Lis1 is underscored by the discovery that haploin-sufficiency of the gene encoding Lis1 causes a smooth brain disorder (lissencephaly) in humans, which is associated with a failure of nuclear migration 42 . Lis1 forms a homodimer, with each monomer comprising an N-terminal dimerization domain and a C-terminal β -propeller domain that binds dynein at the interface between AAA3, AAA4 and the coiled-coil stalk 33,43 (Fig. 1a).

The mechanism by which Lis1 regulates dynein motility remains controversial. In vitro studies on yeast dynein revealed that Pac1, a Lis1 homologue, increases MT affinity, blocks nucleotide-dependent remodelling of the linker domain and markedly reduces dynein velocity^{33,44}. However, the view of Lis1 as a dynein inhibitor is difficult to reconcile with the ability of Lis1 to promote dynein-mediated cargo transport in vivo^{34–41}. Studies on isolated mammalian dynein proposed that Lis1 interacts transiently with dynein, enhances dynein's affinity for MTs on high-load cargos by inducing a persistent-force-generation state^{37,45}. However, the function of Lis1 function is not restricted to high-load cargos, and it is also required for the transport of smaller cargos^{36,38,39,41}. These studies were performed before it was understood that isolated dynein motors are

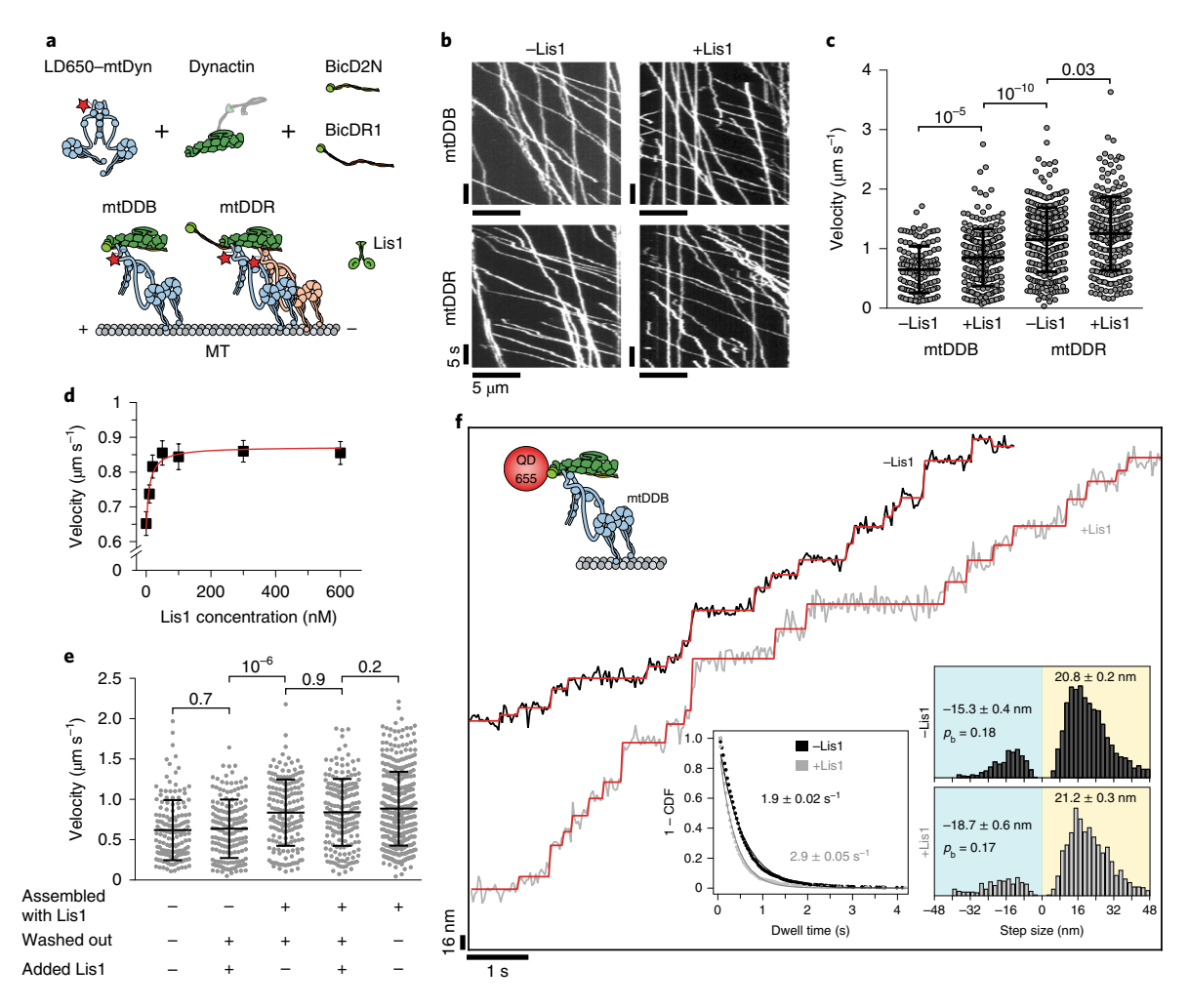


Fig. 1 | Lis1 increases the stepping rate of dynein-dynactin. a, Schematic depiction of the mammalian dynein-dynactin-cargo adaptor complexes. BicD2N primarily recruits single dynein to dynactin (DDB), whereas BicDR1 recruits two dyneins (DDR). Lis1 binds to the dynein motor domain. **b**, Kymographs show the motility of mtDDB and mtDDR on MTs. **c**, Velocity distribution of mtDDB and mtDDR with and without 600 nM Lis1. The centre line and whiskers represent the mean and s.d., respectively. From left to right: n = 132, 217, 307 and 241; mean values are 652, 854, 1155 and 1259 nm s⁻¹, respectively. *P* values are shown. In **a-c**, four independent experiments were performed per condition. **d**. The velocity of mtDDB under different Lis1 concentrations. mtDDB complex was assembled in the presence of Lis1, followed by removing excess protein and introducing Lis1 into the flow chamber. Data are mean ± s.e.m. The red curve represents a fit to a Hill equation with n = 1. From left to right: n = 132, 216, 177, 204, 156, 179 and 217 (three independent experiments). **e**, Velocity distribution of mtDDB assembled in the absence and presence of 600 nM Lis1 under different assembly conditions. The line and whiskers represent the mean and s.d., respectively. *P* values are shown. From left to right: n = 152, 161, 170, 183 and 387; mean values are 622, 638, 838, 842 and 888 nm s⁻¹, respectively (three independent experiments). **f**, Step analysis of quantum-dot (QD)-labelled mtDDB (top right insert) with 2 μM ATP in the presence and absence of 600 nM Lis1. Red staircases represent a fit to a step-finding algorithm. Bottom, left insert: inverse cumulative distribution of dwell times between consecutive steps along the longitudinal axis. Solid curves represent fitting to an exponential decay (decay rate ± s.e.m., n = 2,138 for –Lis1 and 1,441 for +Lis1). Bottom, right insert: normalized histograms of step sizes (n = 2,076 steps for –Lis1 and 1,374 for +Lis1, 6 independent experiments). Average forward and backward

autoinhibited in the absence of dynactin and a cargo adaptor, and may not reflect the force-generation mechanism of active dynein–dynactin complexes^{24,27,46}. In vivo studies gave rise to models in which Lis1 is only required for targeting dynein to the MTs, with dissociation of Lis1 triggering the initiation of transport^{34,38,47–49} and where Lis1 promotes the interaction of dynein and dynactin^{39,40}. Consistent with these models, recent in vitro studies have shown that mammalian Lis1 can increase the frequency and velocity of DDB motility^{49–51}, but the underlying mechanism has remained unknown.

In this study, we determined the effect of Lis1 binding on the motility, stepping and force generation of DDB and DDR using single-molecule imaging and optical trapping in vitro. We found that Lis1 has no substantial effect on the stepping and force generation

of single dyneins after they have associated with dynactin and the cargo adaptor. Instead, Lis1 promotes the assembly of dynein with dynactin. Lis1 also favours the association of two dyneins to dynactin, and this accounts for the increase in both velocity and force generation of the complex. The presence of Lis1 shifts the force balance towards the dynein direction during a tug-of-war with a plus-end directed kinesin. Our work reveals how Lis1 activates the motility of mammalian dynein–dynactin and is therefore required for efficient transport of cargos in cells.

Results

Lis1 increases the stepping rate of dynein-dynactin. We first tested the effect of human Lis1 on the velocity of DDB and DDR

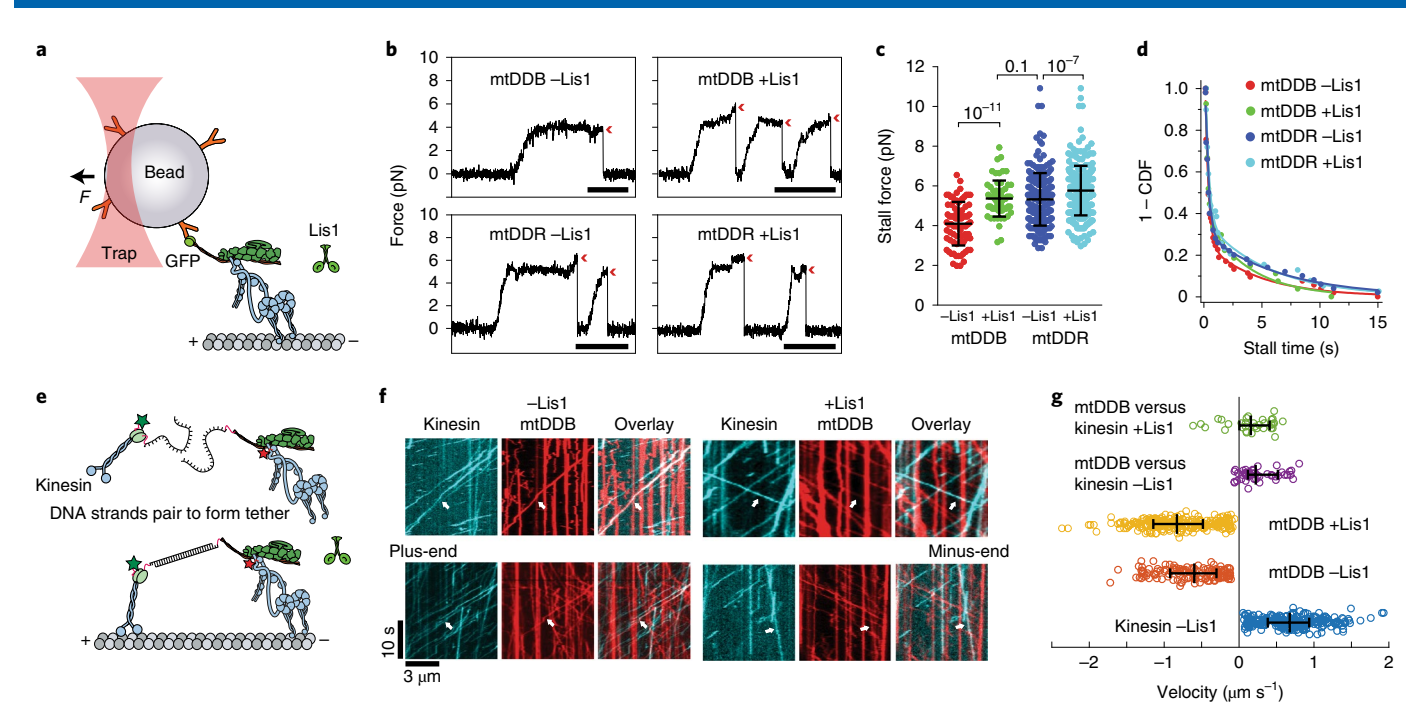


Fig. 2 | Lis1 increases the force production of dynein-dynactin. a, Schematic of a fixed optical-trapping assay for measuring the dynein stall force (*F*). **b**, Typical stalls of beads driven by a single mtDDB or mtDDR. Red arrowheads denote the detachment of the motor from the MT after the stall event. Scale bars, 1s. **c**, Distribution of motor stall forces in the absence and presence of 600 nM Lis1. The centre line and whiskers represent the mean and s.d., respectively. From left to right: n = 80 from 19 beads, 61 from 15 beads, 212 from 38 beads, and 152 from 32 beads; mean values, are 4.1, 5.4, 5.4 and 6.1 pN, respectively. *P* values shown are calculated from a two-tailed *t*-test. In **b,c**, four independent experiments were performed per condition. **d**, Inverse cumulative distribution of stall durations of mtDDB and mtDDR in the presence and absence of Lis1. Solid curves represent fitting to a two-exponential decay (decay time±s.e.m., n = 53, 27, 50 and 39 (left to right, respectively)). **e**, Schematic depiction of the in vitro tug-of-war assay. DDB and kinesin were labelled with different-coloured fluorescent dyes and tethered using a DNA scaffold. **f**, Representative kymographs show the motility of LD650-dynein (red) and TMR-kinesin (green) in the absence and presence of 600 nM Lis1. White arrows show DDB-kinesin colocalizers. **g**, Velocity distribution of mtDDB, kinesin and mtDDB-kinesin assemblies in the absence and presence of Lis1. The centre line and whiskers represent the median and 65% confidence interval, respectively. From top to bottom: n = 33, 45, 217, 132 and 210; median values are 233, 185, -836, -604 and 670 nm s⁻¹, respectively. In **f**, **g**, three independent experiments were performed per condition. Negative velocities represent movement towards the MT minus-end.

complexes assembled with wild-type human dynein (wtDyn), wtDDB and wtDDR, respectively. In agreement with previous measurements 50,51 , wtDDB moved 30% faster in 600 nM Lis1 (two-tailed t-test, $P = 10^{-4}$). We also observed a modest (10%) increase in wtDDR velocity by Lis1 addition (Extended Data Fig. 1). Similar results were obtained using a dynein mutant (mtDyn) that disfavours the autoinhibited phi conformation (Fig. 1a–c and Supplementary Videos 1 and 2). By titrating the Lis1 concentration, we found that 20 nM Lis1 is sufficient for the increased velocity of mtDDB (Fig. 1d). Because mtDyn favours the assembly of active dynein–dynactin complexes the used this construct to study the effect of Lis1 on dynein motility and force generation. Here we designate DDB and DDR complexes formed with mtDyn as mtDDB and mtDDR, respectively.

We altered the order of dynein-dynactin assembly and Lis1 addition to determine whether Lis1 is needed before or after the assembly of mtDDB to increase its speed. First, mtDDB was assembled in the presence of 75 nM Lis1. Removal of excess Lis1 from the flow chamber as the complexes moved along MTs did not lead to slower motility. Second, we assembled mtDDB without Lis1 and removed excess dynein, dynactin and BicD2N from the flow chamber before adding Lis1. The addition of Lis1 after the complexes were being formed had no positive effect on mtDDB speed (Fig. 1e). These results show that Lis1 must be present during the assembly of dynein-dynactin to increase velocity, and that it is dispensable after the complexes walk along the MT.

To distinguish whether Lis1 addition increases dynein step size or stepping rate for faster movement, we determined the stepping behaviour of dynein–dynactin with and without 600 nM Lis1 at limiting (2 μ M) ATP concentrations. We labelled dynein with a bright quantum dot at its N-terminus and tracked the motility of single mtDDB complexes with nanometre precision. In the absence of Lis1, mtDDB has a highly variable step size, frequently taking backward steps³² (Fig. 1f). Lis1 addition did not alter the size and direction of steps taken by dynein. Instead, mtDDB stepped more frequently in the presence of Lis1 (2.9 \pm 0.05 versus 1.9 ± 0.02 s⁻¹; mean \pm s.e.m.; two-tailed *t*-test, $P = 10^{-13}$; Fig. 1f and Extended Data Fig. 2). We concluded that Lis1 increases the dynein stepping rate and not the mean step size, accounting for the faster movement.

Lis1 increases the force production of dynein–dynactin. Using an optical trap, we tested whether Lis1 addition affects the force generation of dynein when this motor forms an active complex with dynactin and a cargo adaptor. We sparsely coated polystyrene beads with BicD2N and BicDR1 adaptors and assembled mtDDB and mtDDR complexes on beads³². Using a fixed trap, we observed that the stall force of mtDDB increases by 22% in 600 nM Lis1 $(4.1\pm0.1 \text{ versus } 5.4\pm0.1 \text{ pN}; \text{ mean}\pm\text{s.e.m.}; \text{ two-tailed } t\text{-test}, P=10^{-11}; \text{ Fig. } 2\text{a-c}$). Lis1 addition also resulted in a modest increase in mtDDR stall force $(5.4\pm0.1 \text{ versus } 6.1\pm0.1 \text{ pN}; \text{ two-tailed } t\text{-test}, P=10^{-4}; \text{ Fig. } 2\text{c}$). Unlike with isolated dynein⁴⁵, we did not observe

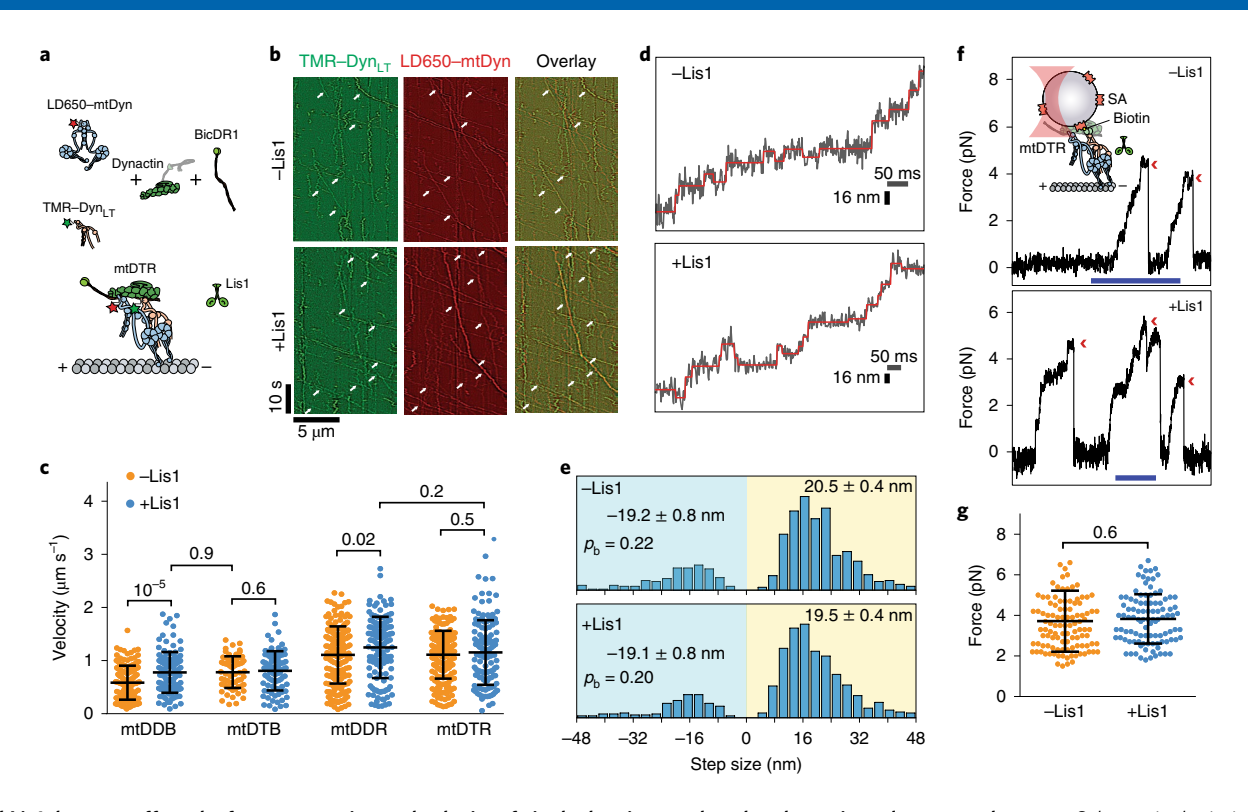


Fig. 3 | Lis1 does not affect the force generation and velocity of single dynein complexed to dynactin and a cargo adaptor. **a**, Schematic depiction of the mtDTR complex. Full-length dynein and Dyn_{LT} are labelled with LD650 and TMR dyes, respectively. **b**, Representative kymographs show the motility of mtDyn and Dyn_{LT}. Arrows represent the colocalization of TMR and LD650. **c**, Velocity distribution of mtDDB, mtDTB, mtDDR and mtDTR in the presence and absence of 600 nM Lis1. The centre line and whiskers represent the mean and s.d., respectively. From left to right: *n* = 144, 117, 65, 88, 209, 134, 213 and 126; mean values are 584, 778, 783, 809, 1108, 1248, 1111 and 1154 nm s⁻¹, respectively. In **b,c**, three independent experiments were performed per condition. **d**, Example traces of beads driven by mtDTR in the presence and absence of 600 nM Lis1 against 1pN hindering force. The raw stepping data are shown in black and the steps fitting are in red. **e**, Normalized histograms of mtDTR steps taken in the longitudinal direction. In **d,e**, *n* = 734 for –Lis1 and 724 for +Lis1 (three independent experiments per condition). Average sizes of steps taken in forward and backward directions (±s.e.m.) and the probability of backward stepping in the presence and absence of Lis1 (shown on graph) are indistinguishable (*P* = 0.6, two-tailed *t*-test). **f**, Top, insert: streptavidin (SA)-coated beads are sparsely decorated with biotin–Dyn_{LT} in the presence of mtDyn, dynactin and BicDR1, and trapped with a focused laser beam. Traces represent typical stalls of beads driven by mtDTR in the absence and presence of 600 nM Lis1. Red arrowheads denote the detachment of the motor from the MT after the stall event. Scale bar, 1s. **g**, Distribution of mtDTR stall force. The centre line and whiskers represent the mean and s.d., respectively. From left to right: *n* = 111 stalls from 23 beads and 101 stalls from 21 beads, and mean values are 3.7 and 3.8 pN, respectively. In **f**,**g**, three independent experiments were perfor

an increase in the stall duration of mtDDB and mtDDR in the presence of Lis1 (Fig. 2d and Extended Data Fig. 3).

We then tested whether the increase in mtDDB force production by Lis1 also increases the probability of DDB winning a tugof-war against a plus-end-directed kinesin-1. We labelled mtDyn and tail-truncated wild-type human kinesin-1 with different fluorescent dyes and pitted one mtDDB against one kinesin-1 using a DNA tether. Consistent with our previous measurements⁴⁶, the majority (87%) of kinesin-DDB assemblies moved towards the plus-end in the absence of Lis1. The median velocity (185 nm s⁻¹ towards the plus-end) was noticeably higher than previous measurements (26 nm s⁻¹) that used a cysteine-light mutant of kinesin-146, probably because the cysteine-light kinesin mutant, but not native kinesin, can be forced to move backwards under resistive forces⁵². The addition of Lis1 increased the percentage of complexes moving towards the minus-end from 13% to 22% and increased the mean velocity of minus-end-moving assemblies by sixfold $(353 \pm 68 \text{ versus } 55 \pm 8 \text{ nm s}^{-1}; \text{ two-tailed } t\text{-test}, P = 0.02; \text{ Fig. 2e-g}$ and Supplementary Video 3). Collectively, these results demonstrate that Lis1 addition increases the likelihood of DDB winning against kinesin in a tug-of-war.

Lis1 does not affect force generation of complexes with a single dynein. We next turned our attention to understanding how Lis1 increases the velocity and force production of mtDDB and mtDDR. To test whether Lis1 alters mechanochemical properties of single dynein assembled with dynactin, we mixed LD650-labelled fulllength mtDyn and a teramethylrhodamine (TMR)-labelled dynein tail construct (Dyn_{LT}) containing residues 1–1,074 of the heavy chain and associated chains)30. Because Dyn_{LT} lacks the motor domain, processive runs of this construct can only be achieved through its side-by-side recruitment with single full-length mtDyn to dynactin. We measured the velocity of dual-labelled complexes that contain both mtDyn and Dyn_{LT} in the presence of BicD2N (mtDTB) and BicDR1 (mtDTR). Lis1 addition did not affect the mean velocity of complexes containing single dynein (Fig. 3a-c and Supplementary Video 4). To test whether Lis1 alters the stepping properties of single dynein bound to dynactin, we tracked beads driven by single mtDTR under a constant 1pN hindering force exerted by the trap. Unlike mtDDB, Lis1 addition did not alter the stepping rate of mtDTR in 1 mM ATP (two-tailed t-test, P = 0.83; Fig. 3d,e and Extended Data Fig. 4a). In addition, Lis1 addition did not affect the stall force and duration (two-tailed t-test, P = 0.6;

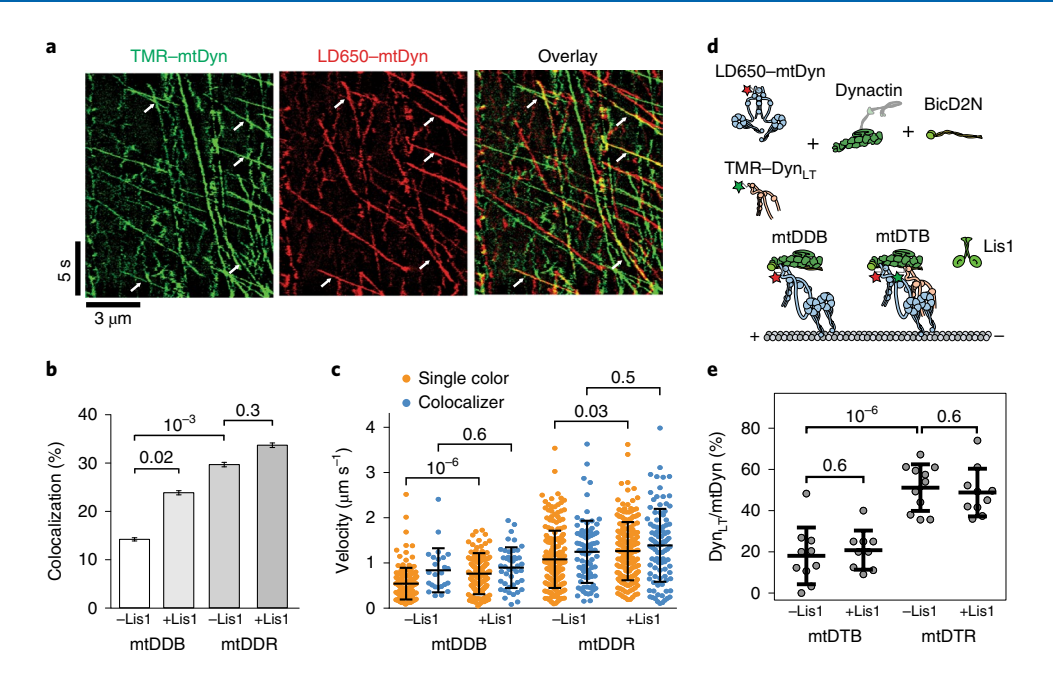


Fig. 4 | Lis1 favours the recruitment of two dyneins to dynactin. **a**, Representative kymographs show the motility of LD650- and TMR-labelled dynein in the presence of dynactin, BicD2N and 600 nM Lis1. Arrows represent TMR and LD650 colocalization. **b**, The percentage of processive complexes that contain both TMR and LD650 signals (mean \pm s.e.m., n = 178, 190, 289 and 290 (from left to right)). Error bars show s.e.m. calculated from multinomial distribution and P values shown are calculated from a two-tailed z-test. **c**, Velocity distribution of single-coloured and dual-coloured complexes of DDB and DDR in the presence and absence of Lis1. The line and whiskers represent the mean and s.d., respectively. From left to right: n = 153, 25, 145, 45, 204, 85, 193 and 97; mean values are 544, 840, 766, 899, 1082, 1248, 1263 and 1390 nm s⁻¹, respectively. P values shown are calculated from a two-tailed t-test. In **a-c**, four independent experiments were performed per condition. **d**, Schematic shows the assembly of mtDDB and mtDTB complexes using TMR-Dyn_{LT}, LD650-mtDyn, dynactin and BicD2N. **e**, The ratio of processive runs by TMR-Dyn_{LT} to LD650-mtDyn on individual MTs in the presence and absence of Lis1. The line and whiskers represent the mean and s.d., respectively (n = 10, 9, 11 and 10 MTs (from left to right), 3 independent experiments). P values shown are calculated from a two-tailed t-test.

Fig. 3f,g and Extended Data Fig. 4b). We concluded that Lis1 does not directly affect the mechanical properties of single dynein bound to dynactin.

Lis1 promotes the recruitment of two dyneins to dynactin. The effect of Lis1 on DDB velocity and force production is highly similar to the recruitment of a second dynein to dynactin^{30,32}, leading us to hypothesize that Lis1 regulates the stoichiometry of dynein and dynactin. To test this possibility, we mixed TMR- and LD650-labelled dynein with dynactin and BicD2N. Dual-coloured complexes contain two dyneins, whereas single-coloured complexes contain either one or two dyneins. Lis1 addition increased the percentage of dual-coloured complexes from 14% to 24% (P = 0.018, two-tailed t-test; Fig. 4a,b and Supplementary Video 5). After correction for labelling efficiency and complexes dual-labelled with the same colour³⁰, we estimated that Lis1 addition increases the percentage of complexes containing two dyneins from 22% to 42%. Consistent with our hypothesis, Lis1 addition did not increase the velocity of dual-coloured complexes that contain two dyneins (Fig. 4c). Similar results were obtained when BicDR1 was used as a cargo adaptor, but the effect of Lis1 addition was modest, presumably because DDR complexes are already predisposed to contain two dyneins³⁰. Collectively, these results demonstrate that Lis1 favours the recruitment of two dyneins to dynactin, which accounts for the higher velocity of these complexes^{30,32,50,51}. We did not observe an increase in the recruitment of Dyn_{IT} side-by-side with mtDyn to dynactin in the presence of Lis1 (Fig. 4d,e and Extended Data Fig. 5), suggesting that Lis1 favours the recruitment of two dyneins to dynactin through its interactions with the motor domain and not with the tail domain^{53,54} of dynein.

Lis1 dissociates from motile complexes. To determine whether Lis1 remains stably bound when dynein moves along MTs⁴⁹⁻⁵¹, we mixed LD650-mtDyn and 50 nM TMR-Lis1 in the presence of dynactin and BicD2N. Thirty per cent of the motile mtDDB complexes contained Lis1. Removal of free Lis1 in assay solution after the initiation of processive motility reduced Lis1-dynein colocalization to 9%, suggesting that Lis1 can dynamically interact with dynein-dynactin as it moves along MTs. In both cases, Lis1-bound complexes had a lower velocity than other mtDDB complexes (Fig. 5a-c and Extended Data Fig. 6a-c). On rare occasions, Lis1 diffused on an MT, hopped onto a motile DDB complex on the same MT (Extended Data Fig. 6d) and slowed down the motility^{33,50}. Therefore, Lis1 typically dissociates from motile complexes but reduces velocity if it remains bound to dynein. These results are not fully consistent with previous reports that Lis1 remains bound to nearly all motile complexes⁵¹ and Lis1-bound complexes have the same velocity⁵⁰ or move faster than complexes that move without Lis151. The disparities may be related to differences in assay conditions and in vitro reconstitution methods.

Stoichiometry of Lis1 binding to dynein is also not well understood. DDB can concurrently recruit two Lis1 dimers⁵⁰. However, it remains unclear whether each of the two dyneins in DDB binds to Lis1, or whether single dynein can simultaneously bind to two Lis1 dimers. To address this, we tested whether two Lis1 molecules could bind to single full-length dynein recruited side-by-side with Atto488-Dyn_{LT} (Fig. 5d). By quantifying DTR complexes colocalized with both TMR-Lis1 and Cy5-Lis1, we estimated that 33% of DTR complexes with at least one Lis1 bound contain two Lis1s (Fig. 5e, Extended Data Fig. 6e and Supplementary Video 6). Recruitment of two Lis1s leads to a further slowdown of the motility compared

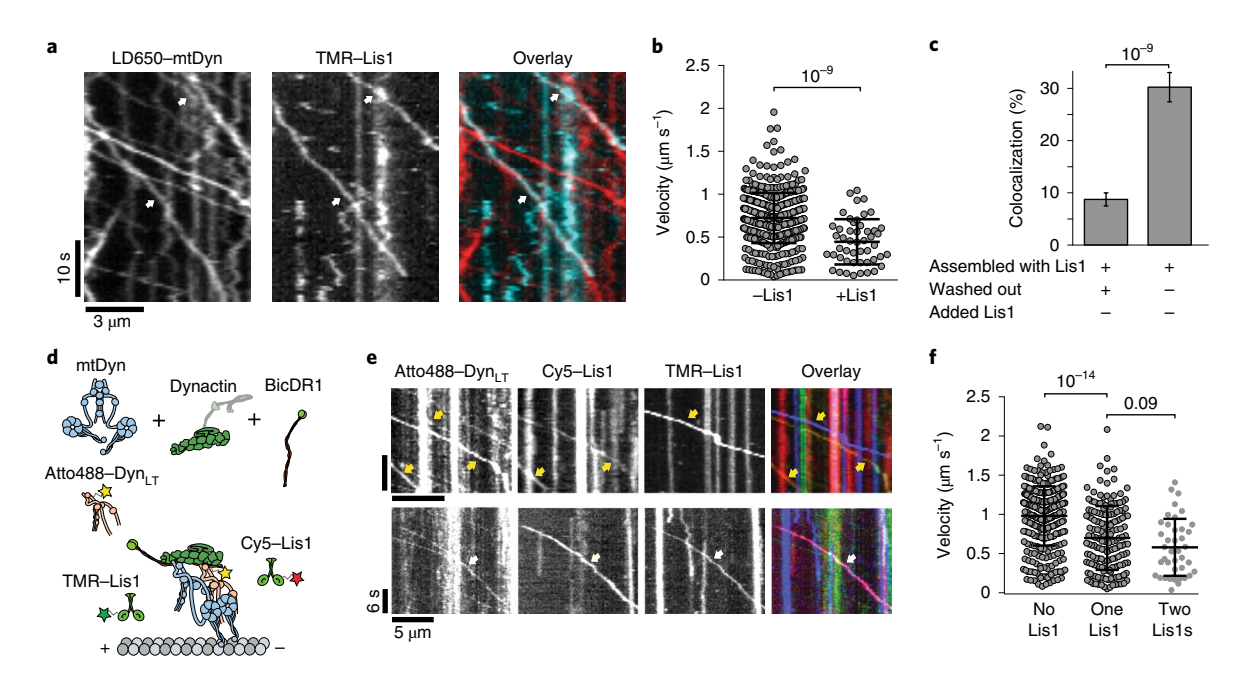


Fig. 5 | Lis1 binding decreases the velocity of dynein-dynactin. a, Representative kymographs show the motility of mtDDB and Lis1 on MTs. White arrows represent the colocalization of LD650-Dyn (red) and TMR-Lis1 (cyan). **b**, Velocity distribution of mtDDB and mtDDB-Lis1 assemblies. The centre line and whiskers represent the mean and s.d., respectively. From left to right: n = 512 and 49; mean values are 726 and 447 nm s⁻¹, respectively. *P* value shown is calculated from a two-tailed *t*-test. In **a,b**, four independent experiments were performed per condition. **c**, The percentage of processive complexes that contain both LD650-mtDyn and Lis1-TMR signals using different assembly conditions (see Methods; mean \pm s.e.m., n = 561 and 387, from left to right, respectively). Error bars represent s.e.m. calculated from multinomial distribution and *P* values shown are calculated from a two-tailed *z*-test. **d**, Schematic depiction of mtDTR complex assembled in the presence of 50 nM TMR-Lis1 and Cy5-Lis1. **e**, Representative kymographs show the motility of mtDTR and Lis1 on MTs. Yellow arrows represent the colocalization of Dyn_{LT} (green) and one colour of Lis1. White arrows represent the colocalization of Dyn_{LT} with Cy5-Lis1 (red) and TMR-Lis1 (cyan). **f**, Velocity distribution of mtDTR that colocalizes with zero, one and two colours of Lis1. The centre line and whiskers represent the mean and s.d., respectively. From left to right: n = 357, 172 and 40; mean values are 985, 701 and 582 nm s⁻¹, respectively. *P* values shown were calculated from a two-tailed *t*-test. In **e**, **f**, three independent experiments were performed per condition.

with single Lis1 (Fig. 5f). These results showed that single dynein can simultaneously recruit two Lis1 dimers.

Lis1 promotes the assembly of active dynein-dynactin complexes. Lis1 stimulates the frequency of minus-end-directed transport under conditions that are insufficient to induce motility, such as when BicD2N concentration is low51. To determine how Lis1 favours initiation of dynein motility when the complex formation is strongly limiting, we quantified wtDDB motility while we lowered the wtDyn concentration 10-, 20- and 50-fold compared with our standard assay condition (see Methods). In the absence of Lis1, the percentage of complexes exhibiting motility was decreased at lower dynein concentrations, and motility was almost fully abolished with the 50-fold dilution. Lis1 addition increased the percentage of motility by approximately fivefold (Fig. 6a,b and Supplementary Video 7), which is consistent with Lis1 favouring association of dynactin with dynein and the BicD2 orthologue in Drosophila cell extracts³⁹. However, when we used mtDyn that does not form the phi conformation, we observed robust motility even in the 50-fold dilution condition and no substantial increase in the percentage of motile complexes with the addition of Lis1 (Fig. 6a,b). We also mixed equal amounts of TMR-wtDyn and LD650-wtDyn with dynactin and BicD2N and quantified the percentage of colocalizing complexes moving along the MTs under limiting dynein conditions (Extended Data Fig. 7). Only around 5% of these complexes were assembled with two dyneins and we did not observe an increase in wtDDB velocity by Lis1 addition (Fig. 6c-e), suggesting that Lis1 promotes motility by recruiting single dynein to dynactin under these conditions. Therefore, Lis1 is also required for the assembly of the first dynein to dynactin, and recruitment of the second dynein does not have to occur together with that of the first dynein.

Discussion

Our results challenge previous views on how Lis1 binding regulates dynein motility. A previous study on isolated dynein suggested that Lis1 binding induces pausing of dynein motility and enhances MT affinity when dynein is subjected to force⁴⁵. Studies on yeast dynein also suggested that Lis1 binding interferes with the power stroke of the linker domain⁴⁴, suggesting that Lis1 binding reduces dynein force generation. Our results with mammalian dynein-dynactin suggest a different mechanism. We found that the presence of Lis1 has no major effect on force generation of single dynein motors bound to dynactin and does not increase the time dynein stalls before dissociating from MTs under resistive loads. Therefore, our results do not support the view that the primary function of Lis1 is to regulate the tenacity of isolated dynein complexes to MTs^{33,44}. Instead, Lis1 favours the recruitment of dynein to dynactin, thereby promoting the assembly of an active complex for dynein motility. This finding explains the requirement for Lis1 for transport initiation in vivo^{34,38}. Consistent with two recent reports that studied the role of Lis1 in mammalian and yeast dynein-dynactin motility^{55,56}, we show that the ability of Lis1 to promote the association of dynein with dynactin also favours the adoption of the two-motor state, which accounts for more frequent stepping and higher force generation per complex. The increased probability of recruiting two dyneins to dynactin also means that Lis1 induces more effective competition against kinesin in a tug-of-war, a result consistent with an increase in anterograde velocity observed when Lis1

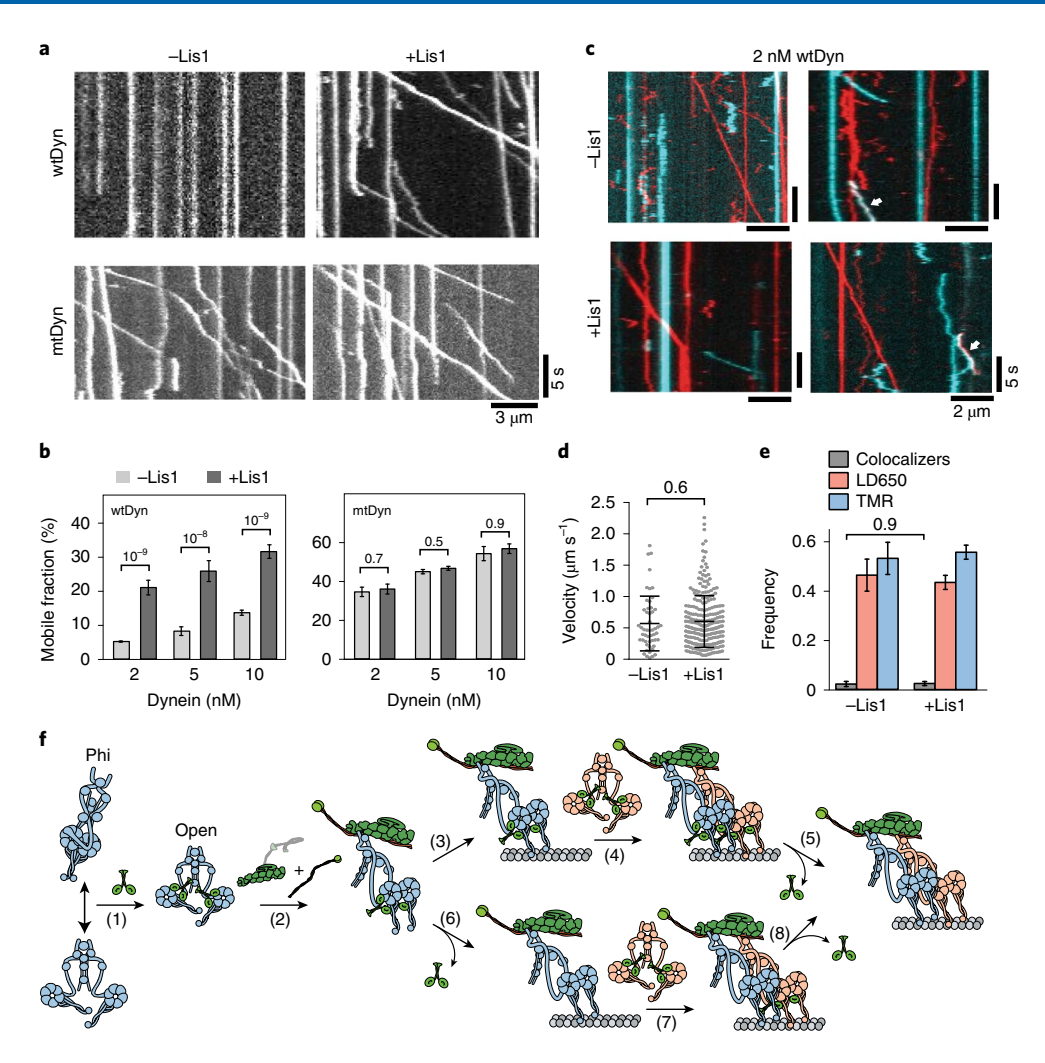


Fig. 6 | Lis1 promotes assembly of the dynein transport machinery. a, Representative kymographs show the motility of DDB at 5 nM concentration of dynein in the absence and presence of 600 nM Lis1. **b**, Ratio comparison of the number of processive runs by DDB to the total number of motors on the MT (mean±s.e.m.). From left to right: n = 508, 355, 491, 262, 1244 and 392 for wtDyn and 234, 459, 426, 1352, 457 and 859 for mtDyn. In **a,b**, three independent experiments were performed per condition. Error bars represent s.e.m. calculated from multinomial distribution and P values shown are calculated from a two-tailed z-test. **c**, Representative kymographs show the motility of LD650-wtDDB (red) and TMR-wtDDB (cyan) at 2 nM dynein in the absence and presence of 600 nM Lis1. Left: single-coloured runs; right: rare events of TMR-LD650 colocalization (white arrows). **d**, Velocity distribution of wtDDB motility assembled at 5 nM dynein in the absence and presence of 600 nM Lis1. The centre line and whiskers represent the mean and s.d., respectively. From left to right: n = 51 and 257; mean values are 572 and 604 nm s⁻¹, respectively. In **c,d**, three independent experiments were performed per condition. **e**, Fraction of processive complexes that contain TMR, LD650 and both TMR and LD650 (mean±s.e.m., n = 59 for —Lis1 and 303 for +Lis1). P values shown are calculated from a two-tailed t-test (**d**) or a two-tailed z-test (**e**). **f**, A model for Lis1-mediated assembly of the dynein-dynactin complex. (1) Lis1 binds to the open conformation of dynein with one Lis1 dimer for each dynein motor domain. (2) Lis1 binding prevents transitions of the open conformation to the phi conformation, which increases the affinity of dynein to dynactin. This mechanism also favours the recruitment of second dynein to the complex, resulting in higher force production and faster movement. Lis1 dissociates from active dynein-dynactin-cargo adaptor motors, either after pairing of two dyneins with dynactin (3-5) or during the asse

is inhibited in cells^{37,39}. Of note, Lis1 does not have to be part of the complex to exert its effects on motility. Lis1 dissociates from most complexes before initiation of movement (Fig. 5), revealing that its primary role occurs during complex assembly. These results also provide an explanation for the recruitment of two dyneins to dynactin observed when the complex was pulled down by BicD2N from brain lysate containing Lis1³¹, in contrast to the recruitment of mostly single dynein when the complex is assembled from purified components in the absence of Lis1³⁰.

Our results provide insights into how Lis1 enhances the affinity of dynein for dynactin. We show that this function is not dependent on reported interactions between Lis1 and the dynein tail, pointing instead to a mechanism that involves binding of Lis1 to the motor

domain. Structural studies on yeast dynein have shown that Lis1 binds to the motor domain at the interface between AAA3, AAA4 and the coiled-coil stalk^{33,43}. Assuming that mammalian Lis1 binds dynein in a similar orientation, Lis1 binding sites are positioned close to the dimerization interface on the AAA+ ring and stalk in the phi particle²¹. We propose that Lis1 binds to the open conformation of dynein and prevents switching back to the phi conformation (Fig. 6f), thereby reducing dynein autoinhibition⁴⁸. Because the open conformation has a higher affinity for dynactin than the phi conformation²¹, Lis1 promotes the assembly of dynein with dynactin and the cargo adaptor and favours the recruitment of two dyneins to each dynactin. The model explains why mtDDB is more likely to have two dynein motors and moves faster than wtDDB in

the absence of Lis1 (Extended Data Fig. 1c,d). The model is also consistent with a recent report that the requirement of Lis1 and NudE in HookA-mediated dynein activation in *Aspergillus nidulans* can be bypassed by expressing mtDyn⁵⁷. Since we obtained a similar increase in the velocity of mtDDB and wtDDB in the presence of Lis1, it is possible that Lis1-bound dynein has additional structural features that are not present in the open conformation and further stimulates the assembly of dynein and dynactin after the opening of the phi conformation. High-resolution structural studies will be needed to determine whether Lis1 binding induces conformational changes on the dynein heavy chain.

Our results are not consistent with a model in which a Lis1 dimer forms a bridge between two dyneins and recruits them simultaneously to dynactin, as we find that Lis1 is required for the assembly of complexes with single dynein at limiting dynein concentrations (Fig. 6 and Extended Data Fig. 7). Moreover, monomeric Lis1, which cannot crosslink two dyneins, also stimulates the assembly of dynein–dynactin, which does not have to occur simultaneously with the second dynein. It remains to be studied whether Lis1 remains bound to dynein motors for the assembly of the fully activated complex, or whether early dissociation of Lis1 from the first dynein could occur before the recruitment of the second Lis1-bound dynein (Fig. 6f).

Mutagenesis studies have indicated that the transition between the phi particle and the open conformation is a tightly regulated process in cells²¹. Future studies will be required to test whether Lis1-mediated opening of the phi conformation is also regulated by other dynein-associated proteins, such as the Lis1-binding proteins NudE and NudEL^{47,58-60}.

Online content

Any methods, additional references, Nature Research reporting summaries, source data, extended data, supplementary information, acknowledgements, peer review information; details of author contributions and competing interests; and statements of data and code availability are available at https://doi.org/10.1038/s41556-020-0501-4.

Received: 17 April 2019; Accepted: 3 March 2020; Published online: 27 April 2020

References

- Roberts, A. J., Kon, T., Knight, P. J., Sutoh, K. & Burgess, S. A. Functions and mechanics of dynein motor proteins. *Nat. Rev. Mol. Cell Biol.* 14, 713–726 (2013).
- Cianfrocco, M. A., DeSantis, M. E., Leschziner, A. E. & Reck-Peterson, S. L. Mechanism and regulation of cytoplasmic dynein. *Annu. Rev. Cell Dev. Biol.* 31, 83–108 (2015).
- Schroer, T. A., Steuer, E. R. & Sheetz, M. P. Cytoplasmic dynein is a minus end-directed motor for membranous organelles. Cell 56, 937–946 (1989).
- Goshima, G., Nedelec, F. & Vale, R. D. Mechanisms for focusing mitotic spindle poles by minus end-directed motor proteins. J. Cell Biol. 171, 229–240 (2005).
- Merdes, A., Heald, R., Samejima, K., Earnshaw, W. C. & Cleveland, D. W. Formation of spindle poles by dynein/dynactin-dependent transport of NuMA. J. Cell Biol. 149, 851–862 (2000).
- Carter, A. P., Diamant, A. G. & Urnavicius, L. How dynein and dynactin transport cargos: a structural perspective. *Curr. Opin. Struct. Biol.* 37, 62–70 (2016).
- Hafezparast, M. et al. Mutations in dynein link motor neuron degeneration to defects in retrograde transport. Science 300, 808–812 (2003).
- Gerdes, J. M. & Katsanis, N. Microtubule transport defects in neurological and ciliary disease. Cell Mol. Life Sci. 62, 1556–1570 (2005).
- Schiavo, G., Greensmith, L., Hafezparast, M. & Fisher, E. M. Cytoplasmic dynein heavy chain: the servant of many masters. *Trends Neurosci.* 36, 641–651 (2013).
- Perrone, C. A. et al. A novel dynein light intermediate chain colocalizes with the retrograde motor for intraflagellar transport at sites of axoneme assembly in *Chlamydomonas* and mammalian cells. *Mol. Biol. Cell* 14, 2041–2056 (2003).

- Gee, M. A., Heuser, J. E. & Vallee, R. B. An extended microtubulebinding structure within the dynein motor domain. *Nature* 390, 636–639 (1997).
- Roberts, A. J. et al. AAA+ ring and linker swing mechanism in the dynein motor. Cell 136, 485–495 (2009).
- Can, S., Lacey, S., Gur, M., Carter, A. P. & Yildiz, A. Directionality of dynein is controlled by the angle and length of its stalk. *Nature* 566, 407–410 (2019).
- Carter, A. P., Cho, C., Jin, L. & Vale, R. D. Crystal structure of the dynein motor domain. Science 331, 1159–1165 (2011).
- Kon, T. et al. The 2.8 Å crystal structure of the dynein motor domain. Nature 484, 345–350 (2012).
- Schmidt, H., Gleave, E. S. & Carter, A. P. Insights into dynein motor domain function from a 3.3 Å crystal structure. *Nat. Struct. Mol. Biol.* 19, 492–497 (2012), S491.
- Vallee, R. B., Williams, J. C., Varma, D. & Barnhart, L. E. Dynein: an ancient motor protein involved in multiple modes of transport. *J. Neurobiol.* 58, 189–200 (2004).
- Bingham, J. B., King, S. J. & Schroer, T. A. Purification of dynactin and dynein from brain tissue. *Methods Enzymol.* 298, 171–184 (1998).
- Torisawa, T. et al. Autoinhibition and cooperative activation mechanisms of cytoplasmic dynein. Nat. Cell Biol. 16, 1118–1124 (2014).
- Walter, W. J., Brenner, B. & Steffen, W. Cytoplasmic dynein is not a conventional processive motor. *J. Struct. Biol.* 170, 266–269 (2010).
- Zhang, K. et al. Cryo-EM reveals how human cytoplasmic dynein is auto-inhibited and activated. Cell 169, 1303–1314 (2017).
- Splinter, D. et al. BICD2, dynactin, and LIS1 cooperate in regulating dynein recruitment to cellular structures. Mol. Biol. Cell 23, 4226–4241 (2012).
- Schlager, M. A. et al. Bicaudal D family adaptor proteins control the velocity of dynein-based movements. Cell Rep. 8, 1248–1256 (2014).
- McKenney, R. J., Huynh, W., Tanenbaum, M. E., Bhabha, G. & Vale, R. D. Activation of cytoplasmic dynein motility by dynactin-cargo adapter complexes. Science 345, 337–341 (2014).
- Ayloo, S. et al. Dynactin functions as both a dynamic tether and brake during dynein-driven motility. *Nat. Commun.* 5, 4807 (2014).
- Urnavicius, L. et al. The structure of the dynactin complex and its interaction with dynein. Science 347, 1441–1446 (2015).
- Schlager, M. A., Hoang, H. T., Urnavicius, L., Bullock, S. L. & Carter, A. P. In vitro reconstitution of a highly processive recombinant human dynein complex. EMBO J. 33, 1855–1868 (2014).
- Schlager, M. A. et al. Pericentrosomal targeting of Rab6 secretory vesicles by Bicaudal-D-related protein 1 (BICDR-1) regulates neuritogenesis. *EMBO J.* 29, 1637–1651 (2010).
- Carnes, S. K., Zhou, J. & Aiken, C. HIV-1 engages a dynein-dynactin-BICD2 complex for infection and transport to the nucleus. *J. Virol.* 92, e00358-18 (2018).
- Urnavicius, L. et al. Cryo-EM shows how dynactin recruits two dyneins for faster movement. *Nature* 554, 202–206 (2018).
- Grotjahn, D. A. et al. Cryo-electron tomography reveals that dynactin recruits a team of dyneins for processive motility. *Nat. Struct. Mol. Biol.* 25, 203–207 (2018).
- Elshenawy, M. M. et al. Cargo adaptors regulate stepping and force generation of mammalian dynein-dynactin. Nat. Chem. Biol. 15, 1093-1101 (2019).
- Huang, J., Roberts, A. J., Leschziner, A. E. & Reck-Peterson, S. L. Lis1 acts as a "clutch" between the ATPase and microtubule-binding domains of the dynein motor. Cell 150, 975–986 (2012).
- Lenz, J. H., Schuchardt, I., Straube, A. & Steinberg, G. A dynein loading zone for retrograde endosome motility at microtubule plus-ends. *EMBO J.* 25, 2275–2286 (2006).
- Stehman, S. A., Chen, Y., McKenney, R. J. & Vallee, R. B. NudE and NudEL are required for mitotic progression and are involved in dynein recruitment to kinetochores. J. Cell Biol. 178, 583–594 (2007).
- Pandey, J. P. & Smith, D. S. A Cdk5-dependent switch regulates Lis1/Ndel1/ dynein-driven organelle transport in adult axons. *J. Neurosci.* 31, 17207–17219 (2011).
- Yi, J. Y. et al. High-resolution imaging reveals indirect coordination of opposite motors and a role for LIS1 in high-load axonal transport. *J. Cell Biol.* 195, 193–201 (2011).
- Egan, M. J., Tan, K. & Reck-Peterson, S. L. Lis1 is an initiation factor for dynein-driven organelle transport. J. Cell Biol. 197, 971–982 (2012).
- Dix, C. I. et al. Lissencephaly-1 promotes the recruitment of dynein and dynactin to transported mRNAs. J. Cell Biol. 202, 479–494 (2013).
- Wang, S. et al. Nudel/NudE and Lis1 promote dynein and dynactin interaction in the context of spindle morphogenesis. *Mol. Biol. Cell.* 24, 3522–3533 (2013).
- Moughamian, A. J., Osborn, G. E., Lazarus, J. E., Maday, S. & Holzbaur, E. L. Ordered recruitment of dynactin to the microtubule plus-end is required for efficient initiation of retrograde axonal transport. *J. Neurosci.* 33, 13190–13203 (2013).

- Moon, H. M. & Wynshaw-Boris, A. Cytoskeleton in action: lissencephaly, a neuronal migration disorder. Wiley Interdiscip. Rev. Dev. Biol. 2, 229–245 (2013).
- 43. DeSantis, M. E. et al. Lis1 has two opposing modes of regulating cytoplasmic dynein. *Cell* 170, 1197–1208 (2017).
- Toropova, K. et al. Lis1 regulates dynein by sterically blocking its mechanochemical cycle. eLife 3, e03372 (2014).
- McKenney, R. J., Vershinin, M., Kunwar, A., Vallee, R. B. & Gross, S. P. LIS1 and NudE induce a persistent dynein force-producing state. *Cell* 141, 304–314 (2010).
- Belyy, V. et al. The mammalian dynein–dynactin complex is a strong opponent to kinesin in a tug-of-war competition. *Nat. Cell Biol.* 18, 1018–1024 (2016).
- Lammers, L. G. & Markus, S. M. The dynein cortical anchor Num1 activates dynein motility by relieving Pac1/LIS1-mediated inhibition. J. Cell Biol. 211, 309–322 (2015).
- 48. Markus, S. M. & Lee, W. L. Regulated offloading of cytoplasmic dynein from microtubule plus ends to the cortex. *Dev. Cell* **20**, 639–651 (2011).
- Jha, R., Roostalu, J., Cade, N. I., Trokter, M. & Surrey, T. Combinatorial regulation of the balance between dynein microtubule end accumulation and initiation of directed motility. *EMBO J.* 36, 3387–3404 (2017).
- Gutierrez, P. A., Ackermann, B. E., Vershinin, M. & McKenney, R. J. Differential effects of the dynein-regulatory factor Lissencephaly-1 on processive dynein-dynactin motility. *J. Biol. Chem.* 292, 12245–12255 (2017).
- 51. Baumbach, J. et al. Lissencephaly-1 is a context-dependent regulator of the human dynein complex. *eLife* **6**, e21768 (2017).
- Andreasson, J. O. L., Milic, B., Chen, G.Y., Hancock, W. O. & Block, S. M. Examining kinesin processivity within a general gating framework. *eLife* 4, e07403 (2015).

- Smith, D. S. et al. Regulation of cytoplasmic dynein behaviour and microtubule organization by mammalian Lis1. *Nat. Cell Biol.* 2, 767–775 (2000).
- Tai, C. Y., Dujardin, D. L., Faulkner, N. E. & Vallee, R. B. Role of dynein, dynactin, and CLIP-170 interactions in LIS1 kinetochore function. J. Cell Biol. 156, 959–968 (2002).
- 55. Htet, Z. M. et al. Lis1 promotes the formation of maximally activated cytoplasmic dynein-1 complexes. *Nat. Cell Biol.* https://doi.org/10.1038/ s41556-020-0506-z (2020).
- Marzo, M. G., Griswold, J. M. & Markus, S. M. Pac1/LIS1 promotes an uninhibited conformation of dynein that coordinates its localization and activity. Nat. Cell Biol. https://doi.org/10.1038/s41556-020-0492-1 (2020).
- Qiu, R., Zhang, J. & Xiang, X. LIS1 regulates cargo-adapter-mediated activation of dynein by overcoming its autoinhibition in vivo. *J. Cell Biol.* 218, 3630–3646 (2019).
- Suzuki, S. O. et al. Expression patterns of LIS1, dynein and their interaction partners dynactin, NudE, NudEL and NudC in human gliomas suggest roles in invasion and proliferation. *Acta Neuropathol.* 113, 591–599 (2007).
- McKenney, R. J., Weil, S. J., Scherer, J. & Vallee, R. B. Mutually exclusive cytoplasmic dynein regulation by NudE–Lis1 and dynactin. *J. Biol. Chem.* 286, 39615–39622 (2011).
- Reddy, B. J. et al. Load-induced enhancement of Dynein force production by LIS1-NudE in vivo and in vitro. Nat. Commun. 7, 12259 (2016).

Publisher's note Springer Nature remains neutral with regard to jurisdictional claims in published maps and institutional affiliations.

© The Author(s), under exclusive licence to Springer Nature Limited 2020

Methods

Protein expression, labelling, and purification. Human SNAPf-wtDyn, SNAPf-mtDyn, SNAPf-Dyn $_{\rm LT}$ (containing residues 1–1074 of the heavy chain), BicD2N-GFP (containing residues 1–400), BicDR1-GFP and Lis1-SNAPf were expressed in Sf9 cells and purified using IgG affinity chromatography (using a cleavable ZZ tag) as described previously^{27,30}. Sf9 cells were regularly tested for mycoplasma infection and no positive results were found. SNAP-tagged proteins were labelled with benzylguanine-functionalized biotin, TMR, Atto488 (NEB) or LD650 probes and purified as described previously³⁰. Dynactin was purified from pig brains using the large-scale SP-sepharose and MiniQ protocol²⁶. Western blotting and mass spectrometry show no detectable levels of Lis1 in dynactin preps (V. Madan and S.L.B., in preparation). Human kinesin-1(1–560)–SNAPf-GFP was expressed in *Escherichia coli* BL21(DE3) cells and purified using Ni-NTA affinity chromatography, as described previously⁶¹. Concentrations of isolated proteins were measured using the Bradford colorimetric assay.

Motility assays. Biotinylated MTs were prepared by mixing 190 μ M of 2% biotin-labelled tubulin with 0.9 mM of unlabelled pig brain tubulin in BRB80 buffer (80 mM PIPES pH 6.8, 1 mM MgCl₂ and 1 mM EGTA), followed by the addition of equal volume of polymerization buffer (2× BRB80 supplemented with 2 mM GTP and 20% anhydrous dimethyl sulfoxide. Tubulin was allowed to polymerize by incubation for 40 min at 37 °C, followed by the addition of 10 nM taxol and incubation for another 40 min. Taxol-stabilized MTs were then pelleted at 20,000g for 12 min and resuspended in BRB80 buffer containing 10 nM taxol and 1 mM dithiothreitol.

The glass surface of motility chambers was first passivated with BSA and functionalized with biotin by flowing 1 mg ml $^{-1}$ BSA–biotin (Sigma) followed by washing the chamber with 40 µl dynein buffer (30 mM HEPES pH 7.0, 5 mM MgSO $_\Phi$ 1 mM EGTA and 1 mM tris(2-carboxyethyl)phosphine) supplemented with 1.25 mg ml $^{-1}$ casein (DB-C). To immobilize biotinylated MTs on the functionalized surface, the chamber was incubated with 1 mg ml $^{-1}$ streptavidin (NEB) and washed with DB-C.

For DDB, DDR and DTR motility assays, $70\,\mathrm{nM}$ LD650–dynein was mixed with 150 nM dynactin and 700 nM cargo adaptor (BicD2N-GFP or BicDR1-GFP) in 10 µl dynein buffer supplemented with 1 mg ml⁻¹ BSA. For DTR experiments, 300 nM TMR-dynein tail was added to the mixture. For dynein-colocalization experiments, 70 nM TMR-dynein was additionally included in the motility mix. The complexes were incubated on ice for 10 min, diluted in DB-C, and flowed into the chamber. The motility mix was kept for 2 min and then washed with $40\,\mu l$ DB-C. To record motility, $20\,\mu l$ dynein motility buffer (DMB) (DB-C supplemented with 1 mM Mg.ATP, 2.5 mM protocatechuic acid and $35\,\mu g\,ml^{-1}$ protocatechuate-3,4-dioxygenase) was introduced into the chamber and the sample was immediately imaged for 3 min at 23 °C. Unless otherwise indicated, experiments with unlabelled Lis1 were performed by mixing Lis1-SNAPf with DDB and introducing the reaction mixture into the chamber. The chamber was then washed with 40 µl DB-C, and Lis1-SNAPf was then reintroduced at the same concentration into the chamber with DMB before recording the motility. In Fig. 5a,b, 50 nM TMR-Lis1 was added to the diluted motility mix (approximately 1 nM LD650-mtDDB) and introduced into the motility chamber. The chamber was then washed with 40 µl DB-C and motility was recorded in the absence of free Lis1 in DMB. In Fig. 5e,f, 50 nM TMR-Lis1 and 70 nM Cy5-Lis1 were incubated with 1 nM Atto488-mtDTR before introducing the mixture into the flow chamber. After washing out unbound proteins from the chamber with 40 µl DB-C, motility was recorded in the absence of free Lis1 in DMB. In Fig. 1e, the role of Lis1 in DDB assembly and motility was tested by introducing and removing Lis1 in different stages of the sample preparation. In Extended Data Fig. 6b,c, 1 nM LD650-mtDDB and 75 nM TMR-Lis1 were introduced into the chamber in DMB containing 75 mM potassium acetate and motility was recorded without washing excess TMR-Lis1 in solution. Although Lis1 has a weak affinity for MTs, this did not affected velocity of dynein-dynactin motility (Fig. 1d).

Single-molecule imaging was performed using a custom-built total internal reflection fluorescence microscope (TIRFM) equipped with a ×100 1.49 numerical aperture Apochromat oil-immersion objective (Nikon) and a perfect focusing system on an inverted microscopy body (Nikon Ti-Eclipse). The fluorescence signal was detected using an EM-CCD (electron-multiplied charge-coupled device) camera (Andor, Ixon EM+). The sample that contained LD650 was excited with a 0.05 kW cm⁻² 633 nm laser beam (Coherent), and the emission signal was filtered using a 655/40 nm bandpass emission filter (Semrock). Videos were recorded using an effective pixel size of 160 nm at 300 ms per frame. For two- and threecolour fluorescence assays, imaging was performed on a multi-colour TIRFM (Nikon) using alternating excitation and time-sharing mode of emission collection. Atto488-, TMR- and LD650-labelled samples were excited using 0.05 kW cm⁻² 488, 532 and 633 nm laser beams (Coherent) and fluorescence signals were detected on an ImagEM X2 EM-CCD camera (Hamamatsu). Videos were recorded at 150 ms per frame per colour for two-colour fluorescence assays and 100 ms per frame per colour for three-colour fluorescence assays. The effective pixel size was 108 nm.

Kymographs were generated from movies in Image J. Processive movement and velocity were then defined and measured as described previously 46 . In brief, kymographs were created by plotting segmented lines along each MT using Image J and individual runs were manually scored. Complexes that were static, diffusive or run shorter than 5 pixels (750 nm) along the MT were excluded from the analysis. In trajectories that exhibit pauses longer than 30 s, only the segments with unidirectional motility were analysed. Pauses shorter than 30 s were included in the analysis. For two-colour imaging, the two channels were overlaid using the merge function. Resulting kymographs were then manually scored for processive events that show colocalization between the two channels. In Figs. 3b and 4a, kymographs were post-processed using the fast Fourier transform function of ImageJ for clarity. Labelling efficiencies of dynein and Lis1 with at least one dye were 96% and 95%, respectively, as determined by spectrophotometry. The fractions of the complexes containing two dyneins or Lis1s were calculated using the colocalization measurements, after accounting for unlabelled complexes and complexes assembled with two dyneins that are labelled with the same colour.

High-resolution fluorescence-tracking assays. Quantum dots were functionalized with benzylguanine by mixing 8 μM amino-(polyethylene glycol) quantum dots emitting at 655 nm (ThermoFisher) with 20 mM benzylguanine–NHS ester (BG-GLA-NHS) (NEB) in 100 mM sodium borate buffer, pH 8.0 for 40 min at room temperature. To remove excess BG-GLA-NHS, functionalized quantum dots were concentrated through five consecutive spins through 100,000 MWCO centrifugal filter units (Amicon). Finally, spin-concentrated quantum dots were suspended in 100 μ l dynein buffer and stored at 4 $^{\circ}$ C.

For tracking the motility of individual dynein complexes, $70\,\mathrm{nM}$ SNAPf-dynein was mixed with 150 nM dynactin, $700\,\mathrm{nM}$ BicD2N–GFP and $600\,\mathrm{nM}$ Lis1–SNAPf in dynein buffer supplemented with 1 mg ml⁻¹ BSA. The complex was incubated on ice for 10 min followed by the addition of 50 nM benzylguanine-functionalized quantum dots for another 10 min in ice. The mixture was then diluted in DB-C and flowed into the motility chamber for 2 min, followed by washing with 80 µl DB-C. Videos were recorded immediately after washing the chamber with 20 µl DMB containing 2 µM Mg-ATP. For tracking the stepping of dynein in the presence of Lis1, $600\,\mathrm{nM}$ Lis1–SNAPf was included in DMB. The sample was excited with a $1\,\mathrm{kW}\,\mathrm{cm}^{-2}$ 488 nm beam (Coherent) and movies were recorded at 30 ms per frame on an Ixon EM+ EM-CCD camera (Andor). For stepping analysis, fluorescence spots of quantum dots were localized using a 2D Gaussian fitting and the resulting trajectories fitted into steps using a custom-written algorithm based on Schwartz information criterion (26.5).

Tug-of-war assays. To prepare a DNA tether between DDB and kinesin, two complementary DNA strands were first functionalized with benzylguanine as described previously. In brief, $25\,\mu M$ DNA oligonucleotides containing an amino group modification at their 5' ends were mixed with 5 mM BG-GLA-NHS (NEB) in 50 mM HEPES buffer containing 50% anhydrous dimethyl sulfoxide, pH 8.5. The reaction was kept overnight at room temperature. The excess unreacted ligand was removed and the benzylguanine-functionalized oligonucleotides were purified by ethanol precipitation of DNA. Finally, isolated DNA was dissolved in dynein buffer and stored at 4°C. The concentration of benzylguanine–DNA was estimated from the absorbance at 260 nm.

BicD2N–SNAPf and kinesin–SNAPf–GFP were labelled with benzylguanine-functionalized oligonucleotides by mixing protein with DNA in dynein buffer for 1 h at 4 °C. DNA and protein concentrations were optimized to yield around 30% efficiency of protein labelling to ensure that the likelihood of dual-labelling of a single dimeric protein with two DNA oligonucleotides was minimized (<9%). The labelling efficiency was quantified by comparing the intensities of labelled to unlabelled bands on 4–12% Bis-Tris SDS–PAGE (Invitrogen). Excess unreacted DNA was removed from BicD2N–SNAPf using a TSKgel G4000SWXL size-exclusion column (Tosoh). In the case of kinesin, a tenfold molar excess of BG-GLA-TMR (NEB) was added to the motor–DNA mixture and the sample was incubated for an additional 30 min at 4 °C. Excess DNA and dye were removed by an MT bind-and-release assay.

In tug-of-war experiments, 200 nM DNA-labelled BicD2N–SNAPf was mixed with 70 nM LD650-labelled dynein and 150 nM dynactin in 10 μ l dynein buffer supplemented with 1 mg ml $^{-1}$ BSA. For experiments with Lis1, 600 nM Lis1–SNAPf was added to the mixture. The mixture was incubated on ice for 10 min, followed by the addition of 150 mM NaCl and 200 nM DNA- and TMR-labelled kinesin–SNAPf–GFP and incubation on ice for a further 20 min. Proteins were then diluted in DB-C and flowed into the chamber, followed by washing with DB-C and imaging in DMB. The buffer was supplemented with 600 nM Lis1–SNAPf in the case of Lis1 experiments.

Optical-trapping assays. For DDB and DDR experiments, complexes assembled with SNAPf-dynein, dynactin and BicD2N-GFP or BicDR1-GFP were mixed with 860-nm-diameter anti-GFP-coated latex beads on ice for 10 min. This assay geometry ensures that beads are driven by active dynein motors assembled to cargo adaptors and eliminates the possibility of cargo-adaptor multimerization. Carboxyl latex beads (860 nm diameter, Life Technologies) were washed and resuspended in activation buffer (10 mM MES, 100 mM NaCl, pH 6.0). The beads were coated by mixing with approximately 2 mg of custom-made polyclonal rabbit anti-GFP antibodies (BioLegend, previously Covance, no. MMS-118P) in activation buffer supplemented with 1 mg each of N-hydroxysulfosuccinimide (Sulfo-NHS) and

1-ethyl-3-(3-dimethylaminopropyl) carbodiimide crosslinkers (Pierce) dissolved in dimethylformamide 64 . The beads were passivated with BSA, washed and stored in PBS supplemented with 0.5 mg ml $^{-1}$ BSA and 0.1% sodium axide at 4 °C. For DTR experiments, SNAPf–Dyn $_{\rm LT}$ was labelled with biotin; and biotin–Dyn $_{\rm LT}$ mtDyn, dynactin and BicDR1 were incubated with 800-nm-diameter streptavidin-coated beads (Spherotech) in ice for 10 min. The protein-coated beads were then diluted in DB-C and flowed into the motility chamber in DMB. The protein concentration in the mixture was gradually reduced in assays until less than 30% of the tested beads exhibited motility activity in contact with Cy5-labelled axonemes to ensure that >95% of the beads are driven by a single complex. For force measurements in the presence of Lis1, 600 nM Lis1–SNAPf was added to the bead-protein mixture and also later added to DMB.

Force measurements were performed on a custom-built optical trap on a Nikon Ti-Eclipse microscope body consisting of a 2W 1,064 nm continuous-wave laser beam (Coherent) and a ×100 1.49 numerical aperture Plan-Apo objective (Nikon), as described previously⁶⁴. Beads were trapped by the laser beam steered by two computer-controlled perpendicular acousto-optical deflectors (AA Electronics). The sample was excited with a 633 nm laser (Coherent) and Cy5-labelled axonemes were imaged using a monochrome camera (The Imaging Source). To detect the bead position relative to the centre of the trap, a position-sensitive detector (PSD, First Sensor) was placed at the back focal plane of a 1.4 numerical aperture oil-immersion condenser (Nikon). Trap stiffness was derived by fitting the power spectrum of a trapped bead that was rapidly raster-scanned in both x and y directions using the acousto-optical deflectors to a Lorentzian spectrum. The typical spring constant used in these experiments was ~0.04 pN nm⁻¹ to allow motors to travel 100-150 nm before stalling. The PSD data were recorded at 20 kHz during calibration and the resulting curve was fit to a cubic polynomial to calibrate the response of the PSD in each sample. For fixed trap assays, PSD data were collected at 5 kHz and downsampled to 500 Hz for ease of visualization. To qualify as a stall event, the bead position should remain stationary for at least 100 ms before rapid (<2 ms) jumping towards the trap centre, implicating release of the motor from the MT. Stall-force histograms were then generated from individual stall events that were manually scored. For force-clamps assays, the PSD signal was acquired at 5 kHz and position feedback was performed at 100 Hz. Beads that walked for at least 100 nm were subjected to force feedback and resulting runs were downsampled to 500 Hz and fit to a step-finding algorithm as described previously⁶⁴. Force-clamp runs that are shorter than 200 nm or included instant jumps larger than 50 nm were excluded from the analysis.

Statistics and reproducibility. At least three independent experiments were performed. Independent experiments showed similar results. The exact number of replicates (*n*) of every dataset is given in the corresponding figure legends. Statistical analysis methods are described in the main text or the figure legend.

Reporting Summary. Further information on research design is available in the Nature Research Reporting Summary linked to this article.

Data availability

All data that support the conclusions are available from the authors on request. Source data for Figs. 1-6 and Extended Data Figs. 1-7 are presented with the paper.

Code availability

Codes used in this paper are available from the corresponding author upon request.

References

- Dogan, M. Y., Can, S., Cleary, F. B., Purde, V. & Yildiz, A. Kinesin's front head is gated by the backward orientation of its neck linker. *Cell Rep.* 10, 1967–1973 (2015).
- DeWitt, M. A., Chang, A. Y., Combs, P. A. & Yildiz, A. Cytoplasmic dynein moves through uncoordinated stepping of the AAA + ring domains. *Science* 335, 221–225 (2012).
- Cleary, F. B. et al. Tension on the linker gates the ATP-dependent release of dynein from microtubules. *Nat. Commun.* 5, 4587 (2014).
- Belyy, V., Hendel, N. L., Chien, A. & Yildiz, A. Cytoplasmic dynein transports cargos via load-sharing between the heads. *Nat. Commun.* 5, 5544 (2014).

Acknowledgements

We thank the members of the Yildiz laboratory for helpful discussions and V. Madan (Medical Research Council) for sharing unpublished results. This work was funded by grants from the National Institutes of Health (GM094522) and National Science Foundation (MCB-1055017 and MCB-1617028) to A.Y., the Medical Research Council (MC_U105178790) to S.L.B. and the Deutsche Forschungsgemeinschaft research fellowship (BA5802/1–1) to J.B.

Author contributions

M.M.E., J.B., S.L.B. and A.Y. conceived the study and designed the experiments. M.M.E. purified dynein, dynactin and cargo adaptors. J.B. purified Lis1 proteins. M.M.E. and E.K. labelled the proteins with DNA and fluorescent dyes and performed the single-molecule motility experiments. M.M.E. and E.K. performed fluorescent tracking assays. M.M.E., S.V. and E.K. performed optical-trapping assays. M.M.E., S.L.B. and A.Y. wrote the manuscript, and all authors read and edited the manuscript.

Competing interests

The authors declare no competing interests.

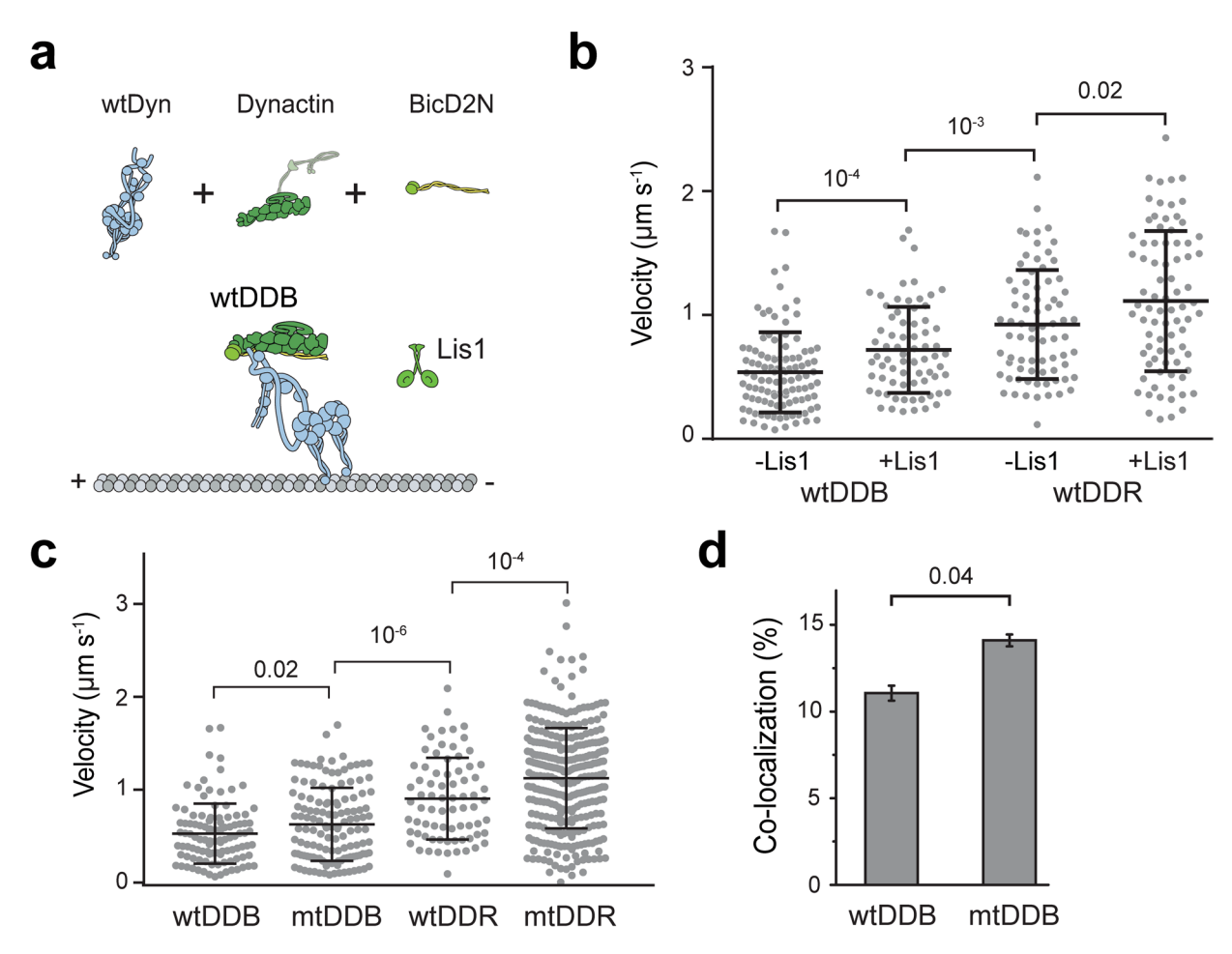
Additional information

Extended data is available for this paper at https://doi.org/10.1038/s41556-020-0501-4.

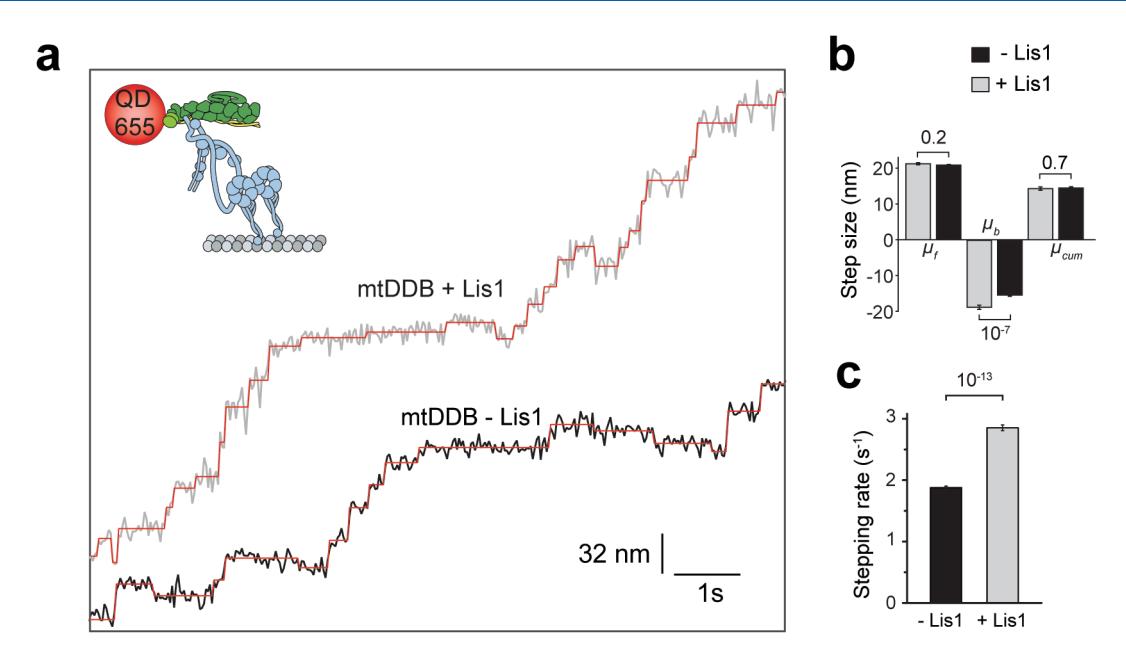
Supplementary information is available for this paper at https://doi.org/10.1038/s41556-020-0501-4.

Correspondence and requests for materials should be addressed to A.Y.

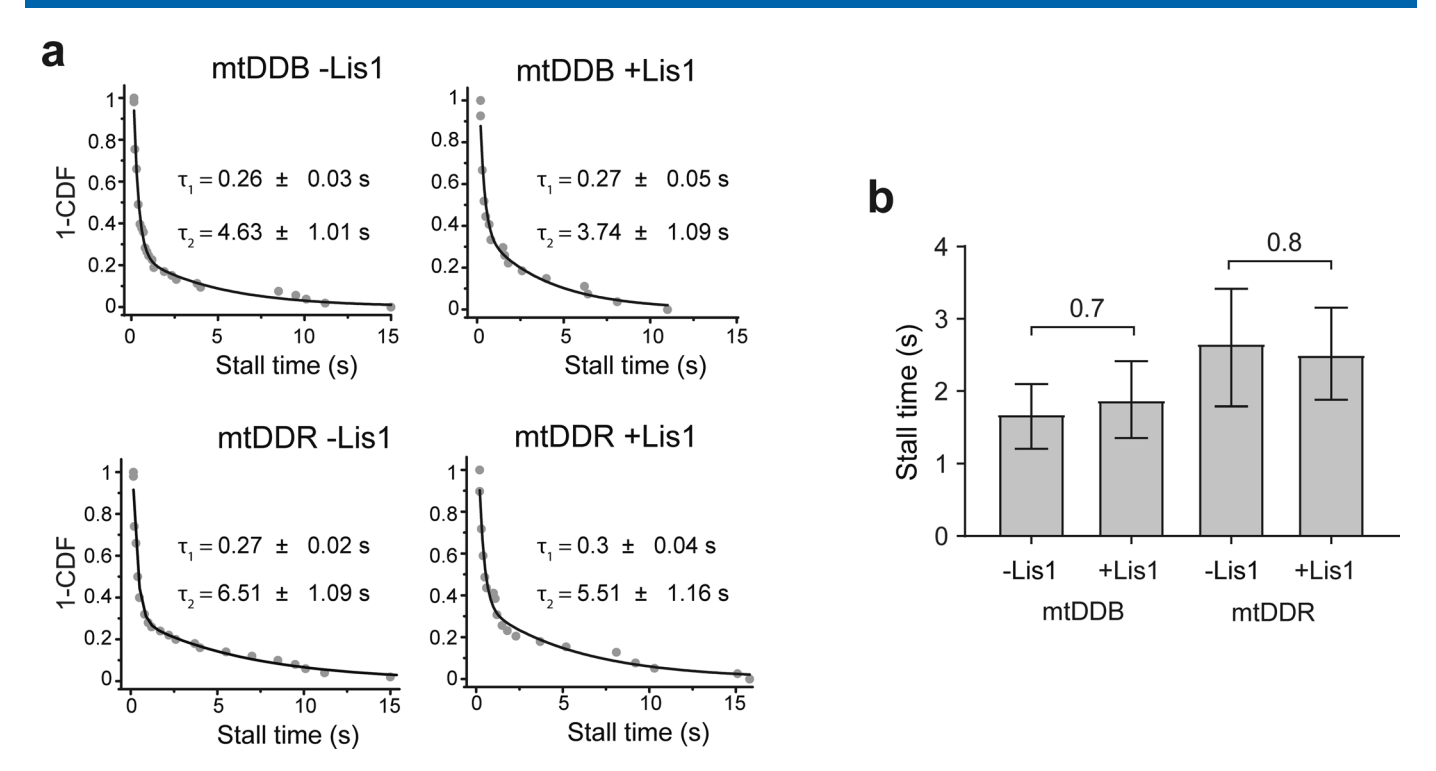
Reprints and permissions information is available at www.nature.com/reprints.



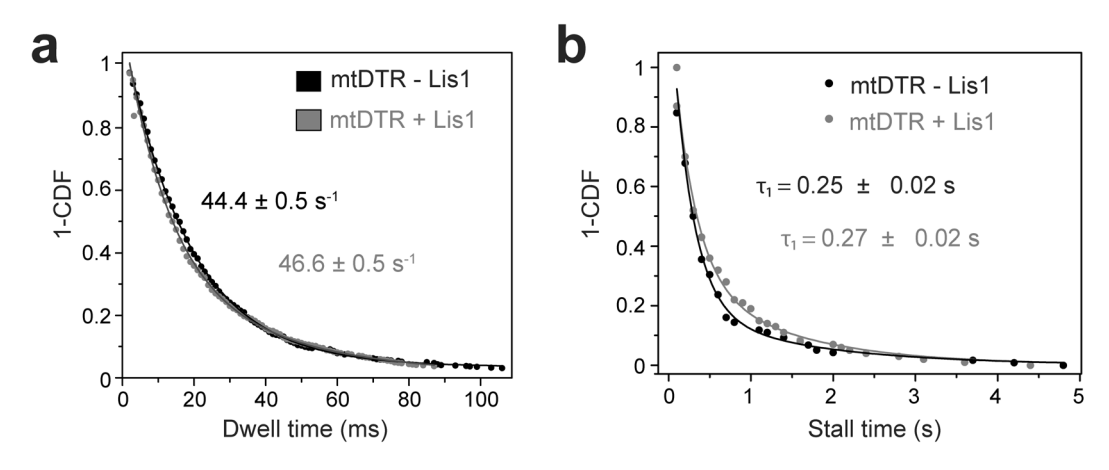
Extended Data Fig. 1 | Lis1 increases the velocity of complexes assembled with wtDyn. a, Assembly of wtDDB and wtDDR. **b**, Velocity distribution of wtDDB and wtDDR complexes assembled in the presence and absence of 600 nM Lis1. The line and whiskers represent the mean and SD, respectively. From left to right, n = 106, 72, 75, and 81, and mean values are 538, 718, 924, 1113 nm s⁻¹ (three independent experiments). p-values are calculated from a two-tailed t-test. **c**, Velocity distribution of complexes assembled with wtDyn and mtDyn in the absence of Lis1. The line and whiskers represent the mean and SD, respectively. From left to right, n = 106, 132, 75, and 307, and mean values are 538, 652, 924, 1155 nm s⁻¹ (three independent experiments). p-values are calculated from a two-tailed t-test. **d**, The percentage of processive wtDDB complexes that are dual-labeled when an equimolar mixture of TMR- and LD650-dynein motors were assembled with dynactin and BicD2N in the absence of Lis1 (mean \pm SEM, n = 246 and 178 from left to right). Error bars represent SE calculated from multinomial distribution and the p-value is calculated from the two-tailed z-test.



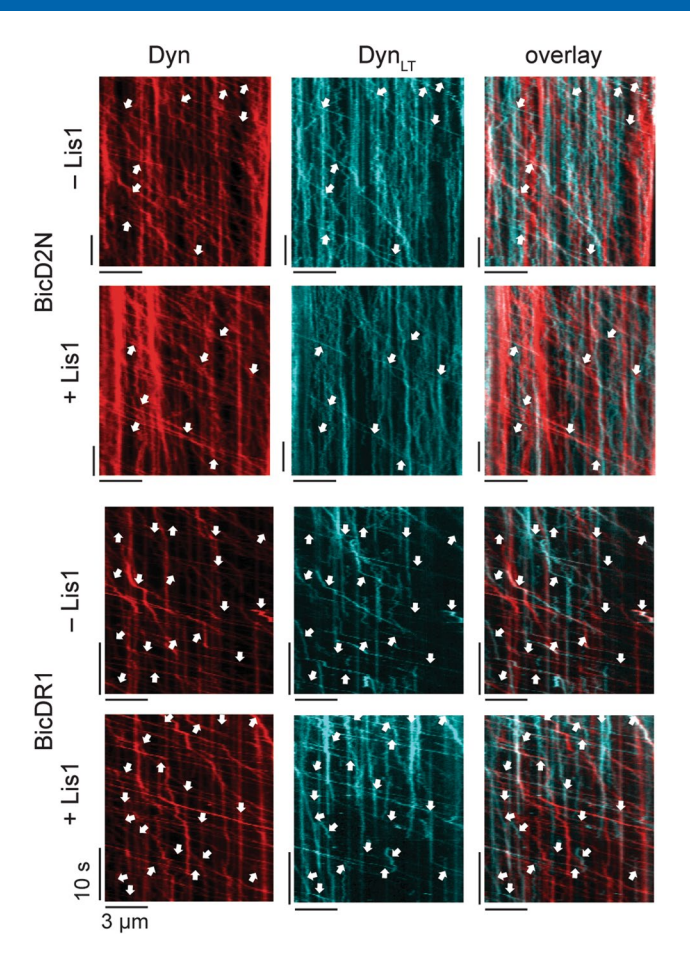
Extended Data Fig. 2 | Step analysis of mtDDB in the presence and absence of Lis1. a, Additional examples of mtDDB stepping in the presence and absence of 600 nM Lis1. **b**, The average size of steps taken in forward (μ_i), backward, (μ_b), and both (μ_{cum}) directions along the longitudinal axis of the MT. Error bars are SEM. In a and b, six independent experiments were performed per condition. **c**, Stepping rates estimated from the exponential fit in Fig. 1f. Error bars are SE of the fit. In b and c, p values are calculated from a two-tailed t-test; sample size (n) distribution of data are provided in Fig. 1f.



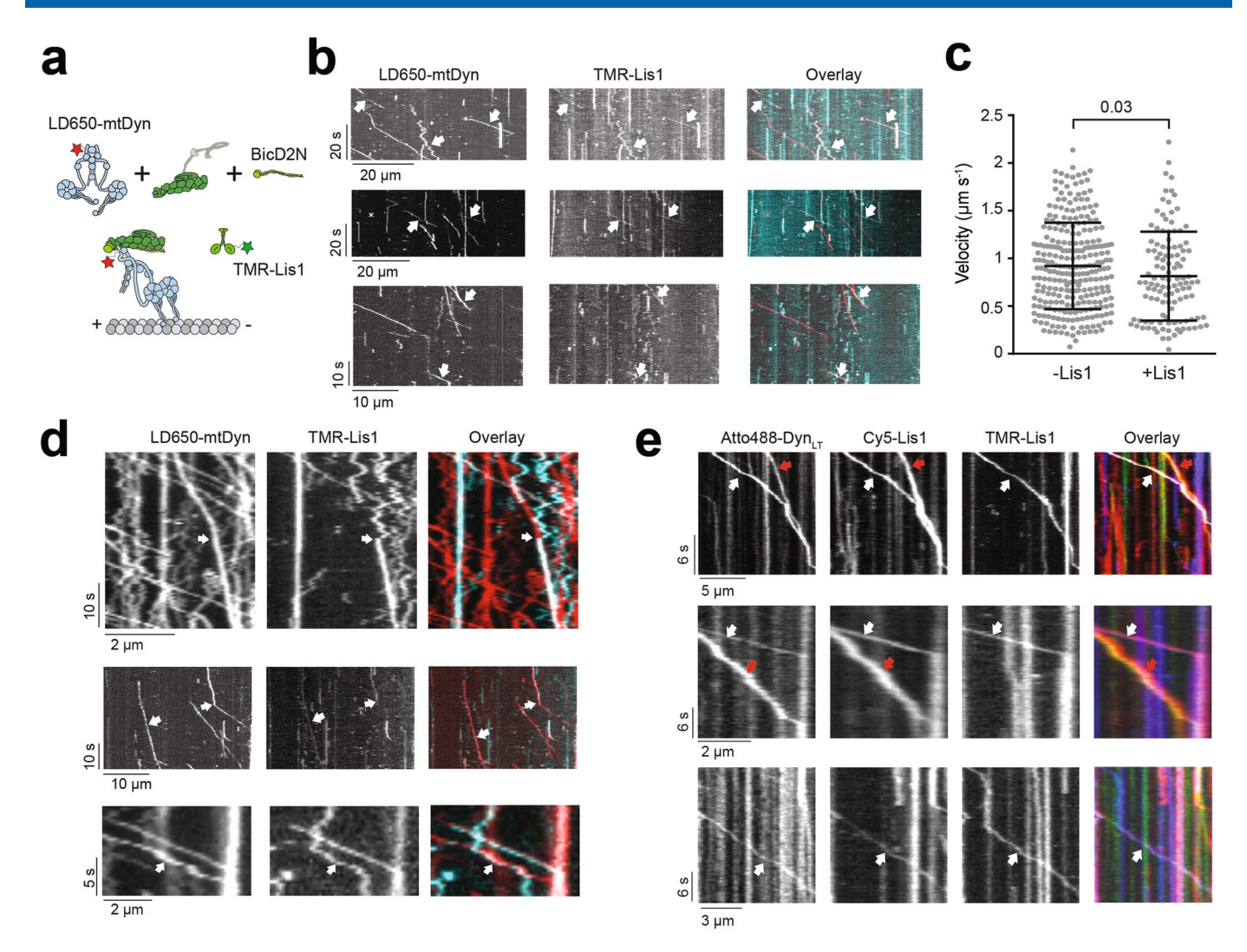
Extended Data Fig. 3 | Lis1 does not increase the stall duration of dynein bound to dynactin and a cargo adaptor. a, Inverse cumulative distribution of stall durations in the absence and presence of 600 nM Lis1. Solid curves represent fitting to a two-exponential decay (decay time \pm SE). b, Mean stall times of mtDDB and mtDDR in absence and presence of 600 nM Lis1 (\pm SEM). p values are calculated from a two-tailed t-test. In a and b, n = 53, 27, 50, and 39 from left to right, four independent experiments per condition.



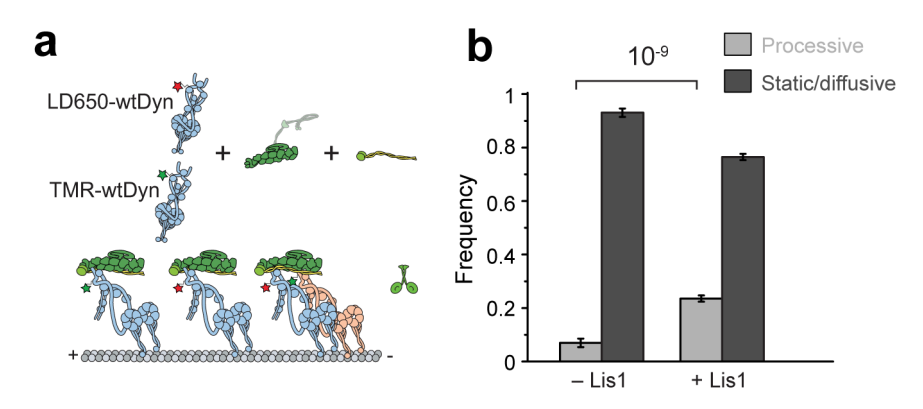
Extended Data Fig. 4 | Lis1 does not affect stall time and stepping rate of single dynein bound to dynactin. a, Distribution of dwell times between consecutive steps along the longitudinal axis of the MT. A fit to an exponential decay reveals the decay rate (rate \pm SE, n = 734 for mtDTR-Lis1 and 724 for mtDTR+Lis1). b, Inverse cumulative distribution of stall durations of mtDTR in the presence and absence of 600 nM Lis1. Solid curves represent fitting to a two-exponential decay (decay time \pm SE, n = 118 for mtDTR-Lis1 and 100 for mtDTR+Lis1, three independent experiments).



Extended Data Fig. 5 | Lis1 does not stimulate the recruitment of dynein tail to dynactin. Representative kymographs show the motility of LD650-Dyn and TMR-Dyn_{LT} assembled with BicD2N or BicDR1 in the presence and absence of 600 nM Lis1. White arrows point to complexes that contain both LD650-mtDyn and TMR-Dyn_{LT} (three independent experiments were performed per condition).



Extended Data Fig. 6 | Additional examples of binding events of Lis1 to mtDDB and mtDTR during processive movement. a, Schematic depiction of mtDDB complex assembled in the presence of TMR-Lis1. b, Representative kymographs show binding of Lis1 to motile mtDDB complexes assembled by mixing 1nM LD650-mtDDB and 75 nM TMR-Lis1 and immediately recording motility with free proteins in solution (see methods). White arrows represent colocalization of LD650-Dyn (red) and Lis1-TMR (cyan). c, Velocity distribution of mtDDB complexes not bound to Lis1 moves faster than complexes that are bound to Lis1 during single-molecule motility. The line and whiskers represent the mean and SD, respectively. From left to right, n = 270 and 117 and mean values are 921 and 813 nms¹. In b and c, three independent experiments were performed per condition. The p-value is calculated from a two-tailed t-test. d, Rare events of dynamic binding of Lis1 to dynein as mtDDB walks along an MT assembled in the presence of 50 nM Lis1. White arrows represent the colocalization of LD650-Dyn (red) and TMR-Lis1 (cyan). In the top kymograph, Lis1 initially diffuses on an MT and then binds to mtDDB during processive movement. Lis1 binding reduces the velocity of the complex. In the middle kymograph, dissociation of Lis1 during mtDDB motility increases the velocity. In the bottom kymograph, a diffusing Lis1 initially binds and later dissociates from mtDDB, without affecting the velocity of the complex (four independent experiments). e, Additional kymographs show single- and dual Lis1 binding to motile mtDTR complexes assembled in the presence of 50 nM Lis1. Red arrows represent the colocalization of Atto488-Dyn_{LT} (green) and Cy5-Lis1 (red). White arrows represent the colocalization of Atto488-Dyn_{LT} (green) with both Cy5-Lis1 (red), and TMR-Lis1 (cyan). Three independent experiments were performed per condition.



Extended Data Fig. 7 | At limiting dynein concentration, Lis1 recruits single dynein to dynactin and BicD2N. a, Schematic depiction of wtDDB assembly using 5 nM LD650-wtDyn and TMR-wtDyn in the absence and presence of 600 nM Lis1. **b**, Fraction of processive and static/diffusive wtDDB complexes on MTs (mean ± SEM, n = 59, 788, 303 and 984 from left to right, three independent experiments).

natureresearch

Corresponding author(s):	Ahmet Yildiz
Last updated by author(s):	Jan 14, 2019

Reporting Summary

Statistics

X Life sciences

Nature Research wishes to improve the reproducibility of the work that we publish. This form provides structure for consistency and transparency in reporting. For further information on Nature Research policies, see <u>Authors & Referees</u> and the <u>Editorial Policy Checklist</u>.

For	all statistical analys	es, confirm that the following items are present in the figure legend, table legend, main text, or Methods section.			
n/a	Confirmed				
	The exact sam	pple size (n) for each experimental group/condition, given as a discrete number and unit of measurement			
	A statement o	on whether measurements were taken from distinct samples or whether the same sample was measured repeatedly			
	The statistical test(s) used AND whether they are one- or two-sided Only common tests should be described solely by name; describe more complex techniques in the Methods section.				
	A description of all covariates tested				
	A description of any assumptions or corrections, such as tests of normality and adjustment for multiple comparisons				
	A full description of the statistical parameters including central tendency (e.g. means) or other basic estimates (e.g. regression coefficient AND variation (e.g. standard deviation) or associated estimates of uncertainty (e.g. confidence intervals)				
	For null hypothesis testing, the test statistic (e.g. <i>F</i> , <i>t</i> , <i>r</i>) with confidence intervals, effect sizes, degrees of freedom and <i>P</i> value noted Give <i>P</i> values as exact values whenever suitable.				
\boxtimes	For Bayesian analysis, information on the choice of priors and Markov chain Monte Carlo settings				
\boxtimes	For hierarchical and complex designs, identification of the appropriate level for tests and full reporting of outcomes				
\square Estimates of effect sizes (e.g. Cohen's d , Pearson's r), indicating how they were calculated					
		Our web collection on <u>statistics for biologists</u> contains articles on many of the points above.			
So	ftware and c	ode			
Poli	cy information abou	ut <u>availability of computer code</u>			
Data collection		Images were acquired using Andor Solis, NIS-Elements, and Ti Control 4.4.2. Labview was used for hardware control of the optical trap setup.			
Data analysis		Tiff images were analyzed using FIJI 1.0. Matlab was used to process and analyze optical trap data and high-resolution tracking assays. Origin Pro 9.0, Matlab, ImageJ, and GraphPad PRISM were used for plotting results.			
		om algorithms or software that are central to the research but not yet described in published literature, software must be made available to editors/reviewers. deposition in a community repository (e.g. GitHub). See the Nature Research guidelines for submitting code & software for further information.			
Da	ta				
All	manuscripts must i - Accession codes, un - A list of figures that	ut <u>availability of data</u> include a <u>data availability statement</u> . This statement should provide the following information, where applicable: ique identifiers, or web links for publicly available datasets have associated raw data restrictions on data availability			
All data that support the findings of this study are available from the corresponding author upon request.					
Fie	eld-speci	fic reporting			

Please select the one below that is the best fit for your research. If you are not sure, read the appropriate sections before making your selection.

Ecological, evolutionary & environmental sciences

Behavioural & social sciences

Life sciences study design

All studies must dis	close on these points even when the disclosure is negative.
Sample size	No pre-specification of sample size was used in the experimental design. In general, no fewer than thirty individual molecules were used to make any conclusions. The sample sizes in our experiments were determined based on previous experiences and relevant publications (Bely, et al. 2016, Nature Cell Biol; Elshenawy et al. 2019, Nature Chem Bio; Generich et al. 2007, Cell)

Data exclusions

The following exclusion criteria were pre-established before data analysis. In fluorescence motility assay, diffusive molecules and molecules with short runs (<750 nm) were excluded from velocity analysis.

In optical trap assays, stalls that are shorter than 100 ms were excluded from analysis. Force-clamp traces that are shorter than 200 nm or that included instantaneous jumps larger than 50 nm were excluded from the analysis.

Replication All experiments were successfully reproduced from at least 3 replicates.

Randomization Randomization was not relevant to this study, because the same protein preparation batch has been used to compare different experimental conditions for each experimental replicate and all trajectories that fit our analysis criteria were included in analysis.

Blinding Investigator analyzing high-resolution tracking assays were not told which sample each stepping dataset belongs to.

Reporting for specific materials, systems and methods

We require information from authors about some types of materials, experimental systems and methods used in many studies. Here, indicate whether each material, system or method listed is relevant to your study. If you are not sure if a list item applies to your research, read the appropriate section before selecting a response.

Materials & experimental systems	Methods	
n/a Involved in the study	n/a Involved in the study	
Antibodies	ChIP-seq	
Eukaryotic cell lines	Flow cytometry	
Palaeontology	MRI-based neuroimaging	
Animals and other organisms		
Human research participants		
Clinical data		

Antibodies

Validation

Antibodies used Custom made anti-GFP antibodies (BioLegend, previously Covance, catalog# MMS-118P) were purified by GFP affinity chromatography to be used for coating carboxyl latex beads (Life Technologies).

Anti-GFP epitope tag antibody was validated and quality-control tested by Western blotting (BioLegend) using Green Fluorescent Protein (GFP, clone B34); https://www.biolegend.com/en-us/products/purified-anti-gfp-epitope-tag-antibody-11364.

Eukaryotic cell lines

Policy information about <u>cell lines</u>	
Cell line source(s)	Sf9 cells were provided by the Cell Culture facility at University of California Berkeley.
Authentication	No cell line authentication was performed.
Mycoplasma contamination	Cells were regulary tested for mycoplasma contamination.
Commonly misidentified lines	No commonly misidentified cell lines were used.